CODEN:LUTEDX/(TEIE-5521)/1-81/(2024)

Industrial Electrical Engineering and Automation

Powertrain System Design for an Ultra-Light Electric Vehicle

Alexander Danielsson

Division of Industrial Electrical Engineering and Automation
Faculty of Engineering, Lund University

Powertrain System Design for an Ultra-Light Electric Vehicle

LUND UNIVERSITY

LTH

FACULTY OF ENGINEERING

Alexander Danielsson

2024

Abstract

This thesis focuses on the optimization of a dual-motor powertrain for an electric vehicle known as the LEVKART, a lightweight four-wheeled vehicle developed for both indoor and outdoor usage. The study examined the effect of different battery voltages, specifically 36 V, 39.6 V, and 43.2 V, on the vehicle's performance. The main focus lies on reducing the energy consumption and increasing the range while adhering to some specific vehicle constraints.

To simulate the vehicle's behavior, a dynamic MATLAB/Simulink simulation model was used. This model was based on an existing one that was modified to better suit the characteristics of the LEVKART. The model incorporated real-world data obtained from motor testing to ensure that the simulations were as realistic as possible. The model was used to simulate various drive cycles and assess the vehicle's behavior during different operational scenarios.

The results from this study provided an initial suggestion for optimizing the powertrain, specifically regarding the most suitable battery voltage for the current electric machine and power electronic components under the specified operating conditions. However, these findings should be interpreted cautiously, as the simulation model would benefit from further work before being fully reliable.

Sammanfattning

Målet med den här studien har varit att optimera drivlinan för ett elfordon kallat LEVKART, ett lättviktigt fyrhjuligt fordon utvecklat för både inomhus- och utomhusbruk. Studien utvärderar olika batterispänningar och deras effekt på fordonets prestanda. Batterispänningarna som kommer att undersökas är 36 V, 39.6 V och 43.2 V. Huvudfokus ligger på att minska energikonsumtionen och öka räckvidden, samtidgt som vissa specifika begränsingar beaktas.

För att simulera fordonets beteende användes en dynamisk MATLAB/Simulink modell. Den här modellen är baserad på en befintlig modell som har anpassats för att bättre representera prestandan och beteendet hos fordonet. Modellen använder sig utav data från motortester för att säkerställa att simuleringarna är så realistiska som möjligt. Modellen användes för att simulera olika körcykler och bedömma fordonets prestanda under olika förhållanden.

Resultaten från denna studie ger en rekommendation på en optimal drivlina, särskilt vilken batterispänning som är mest lämplig tillsammans den nuvarande motorn och kraftelektroniska komponenter under de givna förhållandena. Dessa resultat bör dock tolkas med en viss försiktighet, då simuleringsmodellen fortfarande behöver ytterliggare arbete innan den kan anses vara helt tillförlitlig.

Acknowledgements

I would like to express my deepest gratitude to my supervisor, Mats Alaküla, for his guidance, support, and insightful feedback throughout this project. I am also grateful to the employees at Lund University who assisted me during this work. Special thanks to Getachew Darge and my examiner Avo Reinap, whose expertise was invaluable in helping me navigate the challenges of this thesis.

I would also like to thank my company supervisor, Hannes Bergkvist, and the other employees at LEVTEK, Ivar Bergkvist, and Jake Snowdon, for providing me with the opportunity to apply my academic knowledge in a practical setting and for their valuable insights and support throughout this work.

Alexander Danielsson
Lund, August 2024

Contents

1 Introduction

This chapter aims to provide a brief background on why this thesis topic is relevant and why the optimization of electric vehicle powertrains is important, as well as briefly introduce the specific vehicle on which the optimization is performed.

1.1 Background

The transportation sector is undergoing a pivotal shift from conventional internal combustion engine (ICE) driven vehicles to electric vehicles (EV). The increased popularity of electric vehicles is propelled by a global imperative to reduce carbon emissions and mitigate climate change effects. The European Union has set a target that by 2035, all new cars sold are CO_2 neutral. This initiative is part of the broader legislative package known as *Fit for 55*, which aims to align the EU's climate and energy legislation with the 2030 and 2050 climate objectives [1]. This is a significant step towards ensuring that by 2050, the transport sector can become carbon-neutral.

To meet these goals, it is crucial to optimize our electric vehicles to make them as efficient as possible. Central to the performance of any EV is its powertrain, which includes the electric traction machine, battery, and associated power electronic controls. Optimizing these components for the specific application is essential to improve vehicle performance and efficiency while minimizing cost. Specifically, the overall energy consumption and range are key factors in consumer acceptance and market success. Optimizing the powertrain of electric vehicles and reducing energy consumption can contribute to a reduction in battery size, which in turn can result in an EV with a smaller ecological footprint. A smaller battery not only lightens the vehicle and mitigates the environmental impact, since the manufacturing process of batteries entails a significant ecological footprint, but can also lead to cost reduction and potentially lower the price of the vehicle, making them more accessible.

1.1.1 LEVKART

The LEVKART is a lightweight four-wheeled electric vehicle capable of carrying accessories and loads in various configurations. Developed for both indoor and outdoor usage, the vehicle must be capable of driving at higher speeds (30-40 km/h) to cover longer distances as well as driving at low speeds with high precision in constrained environments. Finding the right balance between fine control, acceleration, speed, and range is crucial to make the vehicle as versatile as possible. The vehicle is powered by two hub motors and a motor controller with monitoring and scripting capabilities.

1.1.2 Trends in Light Electric Vehicles

The market for light electric vehicles is constantly growing. The global market for electric scooters is expected to grow from USD 10.4 billion in 2023 to USD 24.8 billion by 2033 with a CAGR (Compound Annual Growth Rate) of 9.1% [2]. This growth is driven by rising fuel prices, increased environmental awareness, and government initiatives promoting electric mobility. In Sweden alone, over 26 million trips were made with shared electric scooters in 2021 [3].

Given the rising demand and widespread adoption of light electric vehicles, optimizing their powertrain becomes essential for better energy consumption, improved overall vehicle performance, and ensuring that they meet these demands sustainably and efficiently.

Figure 1.1 illustrates a light electric vehicle. It is important to note that this is merely an example of a similar vehicle and not the actual vehicle used in this study. The LEVKART similarly has four wheels and is powered by two PMSM hub motors in the front wheels. However, since the design of the LEVKART has not yet been publicly released, it cannot be illustrated here.

Figure 1.1: Illustration of a light electric vehicle vehicle

1.2 Objective

This thesis aims to contribute to the development of sustainable transport solutions by providing insights into powertrain optimization for light electric vehicles. The objective is to design a dual-motor powertrain where the main focus lies on the choice of battery voltage and energy, power electronics control, and electric traction machine size. The goal is to improve performance and efficiency by optimizing torque and range while adhering to specific vehicle constraints.

A significant aspect of this research is the exploration of different battery voltages and the investigation of the advantages and disadvantages of each system, as each system presents unique implications for the powertrain's efficiency and performance. Specifically, voltage levels of 36V, 39.6V, and 43.2V are investigated. Other aspects that are taken into consideration, are the motor power requirements for different loads and drive conditions, as well as the tradeoff between acceleration, speed, weight, and range.

1.3 Method

In this study, a Simulink model is used to assess various powertrain configurations for the LEVKART, focusing on comparing battery voltages. Specifically, batteries with voltages of 43.2 V, 39.6 V, and 36 V are compared. The model is based on an existing Simulink model, originally designed for other types of electric vehicles, mainly passenger cars, and is modified to reflect the specific characteristics and requirements of the LEVKART. The model ensures that any alterations in components or parameters reflect their impact on the vehicle's overall performance in the simulation model, enabling the simulation of different configurations and applications.

To approximate the real-world behavior of the LEVKART as closely as possible, the traction machine that is being used in the LEVKART today is tested. The resulting data are integrated into the simulation model.

With the simulation model established and validated, various tests are performed to investigate how the energy consumption can be minimized without compromising the performance requirements necessary for the vehicle to operate as intended. The simulation model not only provides a suggestion on an optimal powertrain configuration but also allows for an estimation of the anticipated range of the vehicle, assuming that the drive cycles that are being used are realistic.

2 Modelling and Simulation

This section aims to provide an insight into the optimization process of the vehicle and give an overview of the simulation model and the methods that are used during this process, as well as assumptions and estimations that are made.

2.1 Simulation Model

A comprehensive and dynamic simulation model is developed to thoroughly examine the vehicle's behavior under different configurations and optimize its powertrain. The simulation model is based on an existing Simulink model from Professor Mats Alaküla's course on Electric and Electric Hybrid Vehicle Technology, which is modified to suit the specific characteristics of the LEVKART. The course material, including equations from the Simulink model along with [4], is used to present the mathematical expressions involved in developing the new model and its parameters. This updated model serves as the foundation for investigating the vehicle's performance across a range of driving conditions, enabling a holistic understanding of its efficiency, range, and overall dynamics. The simulation model consists of several subsystems, each representing the real-world behavior of the vehicle's components. An overview of the Simulink model is shown in figure 2.1. The optimization process primarily targets the battery, electric traction machine, and power electronics, making these subsystems the focal point of the simulations, which are further presented in section 2.3, 2.4, and 2.5. The simulation is performed with drive cycles specifically designed to represent the unique operational scenarios anticipated for this vehicle, ensuring realistic and relevant simulations.

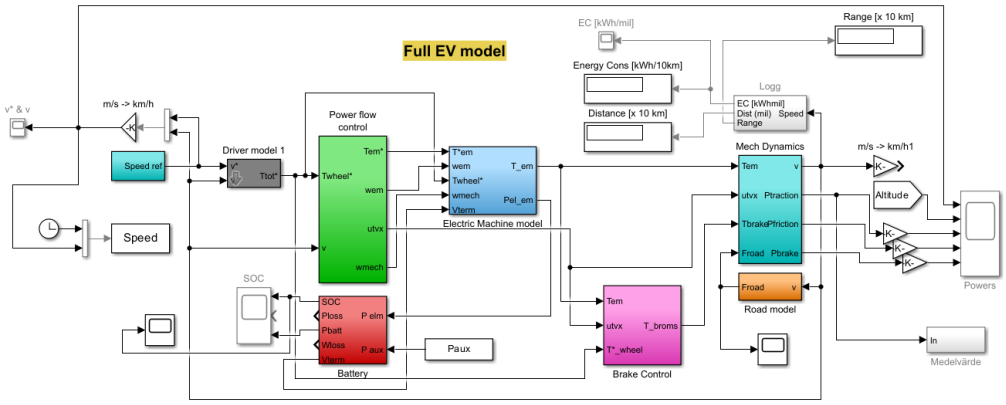

Figure 2.1: The Simulink model used during the simulations

2.2 Simulation Strategies

Optimizing the powertrain for an electric vehicle requires a detailed understanding of vehicle dynamics and drivetrain performance under various driving conditions. This study draws on methodologies from [5], which used MATLAB/Simulink to simulate the battery performance across different urban driving cycles. This study focused on achieving realistic urban driving simulations, and their findings show how varying drive cycles impact battery utilization and the range of the vehicle, emphasizing the importance of simulating multiple drive cycles and evaluating if the results differ between them. This is particularly crucial when simulating the driving behavior and the expected range of the LEVKART, which is intended for applications lacking established drive cycles. This makes it harder to simulate how the vehicle can be used and makes it important to compare different drive cycles that might affect the performance of the vehicle differently. If the vehicle is used in urban environments, there is more data available that might correspond better to the actual drive pattern of the LEVKART. In industrial use cases, like transportation within a factory or warehouse, this is more complicated and the drive patterns are estimated as well as possible.

The absence of official test cycles for similar light electric vehicles is discussed further in [6], which describes a study on the optimal design of electric micro-mobility vehicles. They use custom drive cycles that were measured by completing a representative driving mission and logging the data with a GPS-based application to get realistic cycles. Although this method is possible to some extent for the LEVKART, it might not be completely representative as some assumptions about the driving patterns would still have to be made in these applications intended for the LEVKART.

Due to the lack of established drive cycles for this type of vehicle, existing cycles for other vehicles are adapted to represent the anticipated usage patterns of the LEVKART. These cycles are scaled to match the LEVKART's top speed of 35 km/h and adjusted to align with its acceleration capabilities, ensuring that they accurately represent the vehicle's performance characteristics. This process is further described in section 2.7.

2.3 Battery Model

The battery subsystem simulates the behavior of the vehicle's battery pack during the drive cycle. This includes calculating losses due to internal resistance and using a discharge curve to represent the battery's voltage drop throughout the entire drive cycle. The discharge curve is retrieved from a datasheet for a specific battery cell, called Samsung INR18650-29E 2900 mAh. Figure 2.2 shows the discharge curve for this specific cell [7]. The different colors in the figure represent the voltage drop across different constant discharge currents, ranging from 0.2 A to 7.0 A. The curves labeled 'A' and 'B' for each discharge current represent repeated tests for each current level, intended to demonstrate the consistency of the battery's performance.

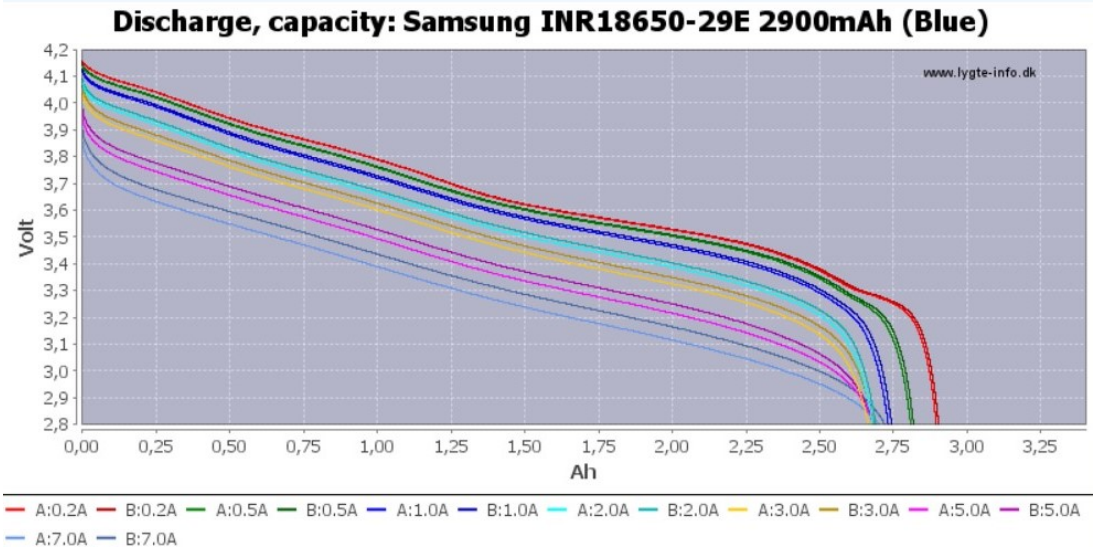

Figure 2.2: Discharge curve for Samsung INR18650-29E 2900 mAh battery cell

Figure 2.3 shows the discharge curve for three different battery packs. The 43.2 V battery uses the Samsung INR18650-29E cell and is currently used in one of the prototype vehicles. The values of the curves in figure 2.2 were not available. Therefore, the image of the discharge curve is traced and recreated in Matlab to obtain necessary data points, as detailed in Appendix A.1. Although this method is not perfectly accurate, it is the most practical approach due to the lack of raw data. A curve from the middle range is selected to represent the battery pack's discharge current under typical operating conditions, as this reflects a balanced view of the performance for the expected power demands. The scale on the y-axis in figure 2.3 is adjusted to start at the charging voltage, expressed in volts, for each one of the batteries, while the overall shape of the curve remains constant. The x-axis represents the SoC (State of Charge) expressed in percentages.

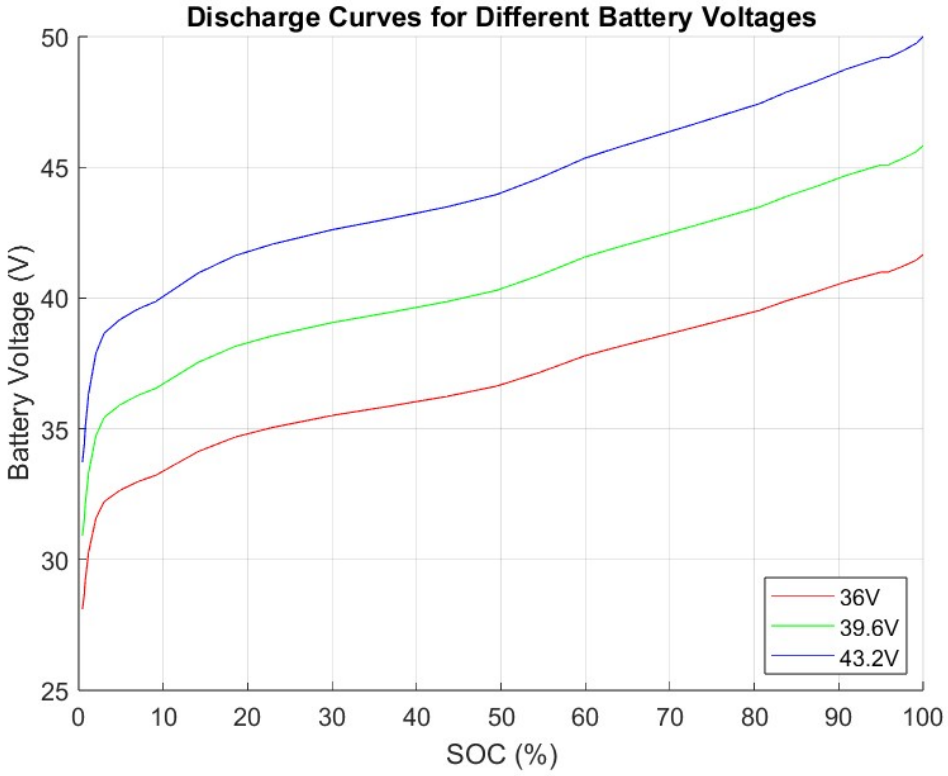

Figure 2.3: Discharge curves for the 36 V, 39.6 V, and the 43.2 V battery packs

The 43.2 V battery has a 12s3p (12 series 3 parallel) cell configuration [8]. This battery is used as a reference, as this is the battery pack currently used in the LEVKART. To compare the performance at different voltages while maintaining energy content close to the 376 Wh of the 43.2 V battery, two additional batteries are designed, using the same Samsung cells as the 43.2 V battery: a 39.6 V battery with an 11s3p configuration and a 36 V battery with a 10s4p configuration. The specifications for all three batteries are listed in table 2.1. The Samsung cells used in each one of these batteries have a nominal capacity of 2900 mAh, a nominal voltage of 3.6 V, and a charging voltage of 4.2 V. The decision to use these cells stems from the fact that the 43.2 V battery pack, which uses these cells, is already in use in the prototype vehicle.

Rated Voltage	**43.2 V**	**39.6 V**	**36 V**
Battery Configuration	12s3p	11s3p	10s4p
Capacity	8.7 Ah	8.7 Ah	11.6 Ah
Charging Voltage	50.4 V	46.2 V	42 V
Energy	376 Wh	345 Wh	418 Wh
Resistance	0.24 Ω	0.22 Ω	0.15 Ω

Table 2.1: Specifications for the batteries

2.3.1 Battery Type

The battery pack that is being simulated is a lithium-ion battery. These batteries are well-suited for electric mobility solutions due to their superior energy density and long life length. They can maintain a high voltage throughout the discharge cycle, providing uniform output power, which is essential for maintaining optimal performance during varying urban conditions. Another key advantage of lithium-ion batteries is their charging and discharging efficiencies, which can reach up to 95%, significantly contributing to the overall energy efficiency of the vehicle [9]. The battery currently used in the LEVKART prototype is a 43.2 V lithium-ion battery with the battery cells mentioned in section 2.3 and discharge curve according to figure 2.3.

2.4 Power Electronics Model

To accurately reflect the vehicle's performance throughout the drive cycle, the simulation incorporates a power electronics model that calculates the losses and efficiencies of the power electronic components. In this model, the efficiency of the power electronics is calculated based on instantaneous operational parameters such as the battery voltage, which is determined from the discharge curve using the SoC. The equations used in this part are retrieved from the old Matlab model.

$$P_{T,sw} = \frac{2\sqrt{2}}{\pi} \cdot \frac{E_{on,n} + E_{off,n}}{V_{dc,n} \cdot I_n} \cdot V_{dc} I_i f_{sw} \tag{2.1}$$

$$P_{D,sw} = \frac{2\sqrt{2}}{\pi} \cdot \frac{E_{Drr,n}}{V_{dc,n} \cdot I_n} \cdot V_{dc} I_i f_{sw} \tag{2.2}$$

$$P_{T,cond} = (\frac{\sqrt{2}}{\pi} \cdot V_{T0} I_i + \frac{1}{2} \cdot R_{T(on)} I_i^2) + (V_{T0} I_i + \frac{4\sqrt{2}}{3\pi} \cdot R_{T(on)} I_i^2) \cdot \frac{U_i cos(\varphi)}{V_{dc}} \tag{2.3}$$

$$P_{D,cond} = (\frac{\sqrt{2}}{\pi} \cdot V_{D0} I_i + \frac{1}{2} \cdot R_{D(on)} I_i^2) - (V_{D0} I_i + \frac{4\sqrt{2}}{3\pi} \cdot R_{D(on)} I_i^2) \cdot \frac{U_i cos(\varphi)}{V_{dc}} \tag{2.4}$$

The total losses are calculated in equation 2.5 as a sum of equation 2.1, 2.2, 2.3 and 2.4, that account for both conduction and switching losses within the power electronics components. The efficiency is calculated in equation 2.6. The losses, and consequently the efficiency, are calculated across a range of values to create an efficiency map. This efficiency map is implemented in the Simulink model and used with different voltage levels and currents. This means that the efficiency is calculated dynamically, and the efficiency of the power electronics components varies according to the battery voltage. How these calculations are performed in Matlab is detailed in Appendix A.1.

$$P_{loss} = P_{T,sw} + P_{D,sw} + P_{T,cond} + P_{D,cond} \tag{2.5}$$

$$Efficiency = \frac{P_{out}}{P_{out} + P_{loss}} \tag{2.6}$$

All parameters required for the equations above are retrieved from a datasheet for the specific components used in the LEVKART [10]. Table 2.2 presents the parameters that are extracted from this datasheet.

Parameter	**Value**	**Parameter**	**Value**
V_{to}	0.19 V	E_{on}	5.14e-6 J
V_{do}	0.23 V	E_{off}	5.14e-6 J
$R_{t(on)}$	0.17e-3 Ω	$V_{dc,n}$	60 V
$R_{d(on)}$	0.01 Ω	I_n	36 A
$E_{d(rr)}$	1.62e-6 J		

Table 2.2: Parameters retrieved from the datasheet

2.4.1 Efficiency Map

The efficiency map is presented in a matrix that correlates efficiency with varying currents and voltage levels. The efficiency map also accounts for another variable, the power factor $cos(\varphi)$, which changes dynamically throughout the drive cycle. The efficiency maps are stored in a three-dimensional matrix, which is used in the Simulink model along with a lookup table that extracts the corresponding efficiency at a specific time. This lookup table has three input signals: current, voltage, and $cos(\varphi)$. These input parameters are all calculated dynamically, ensuring the most accurate simulations possible at any given moment during the drive cycle.

Figure 2.4 shows an efficiency map for the power electronic components used in the LEVKART as a function of current and voltage. This efficiency map corresponds to $cos(\varphi) = 1$. Figure 2.5 shows the corresponding contour maps for the efficiency of the power electronic components.

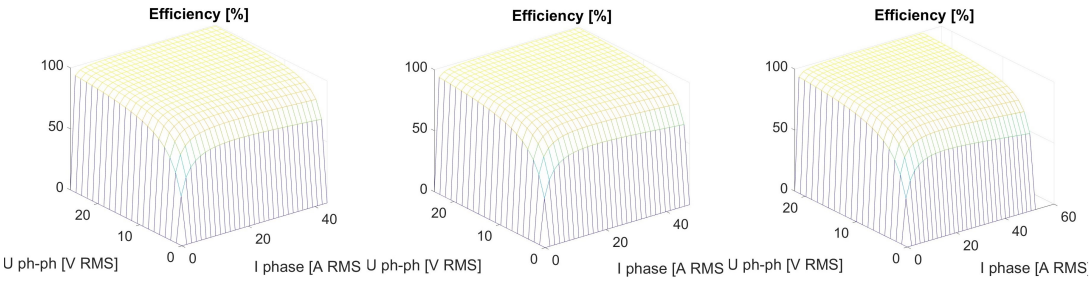

Figure 2.4: Efficiency as a function of the current and the voltage, $cos(\varphi) = 1$ - from left to right: 43.2 V, 39.6 V, 36 V

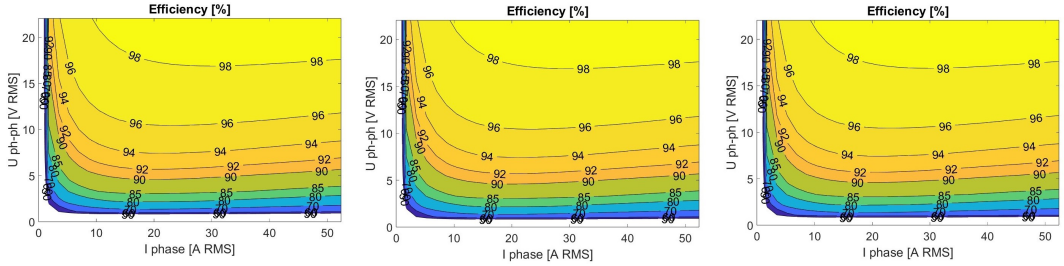

Figure 2.5: Contour maps of the efficiency - from left to right: 43.2 V, 39.6 V, 36 V

2.5 Electric Machine Model

To calculate the losses in the electric machine a similar approach is used as in section 2.4, where the efficiency for the power electronic components is being calculated. The efficiency of the electric machine is calculated according to equations 2.7, 2.8, 2.9, 2.10 and 2.11, which is retrieved from the original Simulink model that this study is based upon. This is a simplified model for an electric traction machine that calculates an approximate efficiency map based on the desired performance parameters, such as maximum power, maximum speed, and maximum torque.

$$Efficiency = \frac{P_{axle}}{P_{electric} + P_{loss,resistive} + P_{loss,magnetic}} \tag{2.7}$$

$$P_{axle} = T \cdot \omega \tag{2.8}$$

$$P_{loss,resistive} = R_s \cdot I_s^2 \tag{2.9}$$

$$P_{loss,magnetic} = P_{max} \cdot 0.02 \cdot (\frac{\psi_s}{\psi_{s,max}})^2 \tag{2.10}$$

$$P_{electric} = -\omega \cdot \psi_{sy} \cdot i_{sx} + \omega \cdot \psi_{sx} \cdot i_{sy} \tag{2.11}$$

In the equations above, R_s is the stator resistance. I_s is calculated with the currents i_{sx} and i_{sy}, using the formula $I_s = \sqrt{i_{sx}^2 + i_{sy}^2}$, and ψ_s is the magnetic flux linkage. The resulting efficiency matrix is used with a lookup table to extract the efficiency at any given time during the drive cycle. Two input signals are needed, the torque and the speed. Both of these parameters vary throughout the drive cycle, leading to a dynamically changing efficiency.

Figure 2.6 shows an efficiency map for an electric machine, illustrating how the efficiency varies with torque and speed. The blue line represents the optimal operating point for the machine, while the red line indicates the torque limit at different speeds.

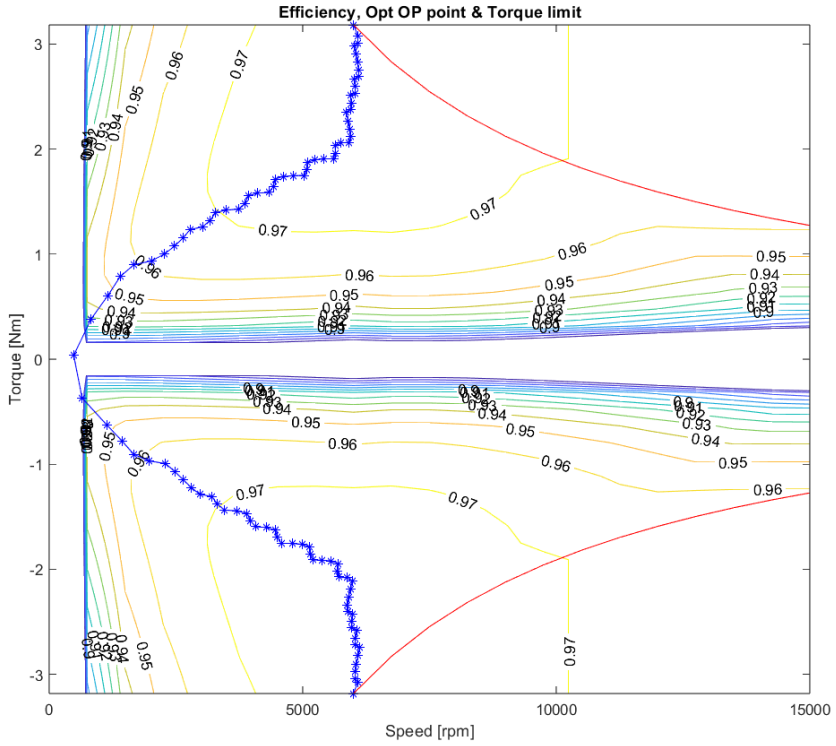

Figure 2.6: Efficiency map for an electric traction machine

2.6 Input Parameters

The current used as input to the lookup table is a function of the direct axis current i_d and the quadrature axis current i_q, or i_{sx} and i_{sy}, according to equation 2.12. The voltage used as an input is the stator voltage, which is calculated using formula 2.13. These parameters vary throughout the drive cycle and is calculated dynamically. i_{sx} and i_{sy} depends on the torque T and the stator flux linkage ψ_s, which is the input to the lookup tables that determine the currents. ψ_s is calculated using the formula 2.14, where u_{batt} represents the battery voltage, which changes according to the discharge curve for the cell that is discussed in section 2.3.

The electrical angular velocity, ω_{el}, is a function of the mechanical angular velocity, ω_{mech}, and is calculated with formula 2.15. In this equation, P represents the number of poles, which is 40 in this machine.

The input signals needed to extract the stator voltage and the power factor $cos(\varphi)$ in the Simulink model are torque T and ω_{el}.

$$I_{ph,rms} = \sqrt{i_{sx}^2 + i_{sy}^2} \tag{2.12}$$

$$U_{ph-ph,rms} = \frac{1}{\sqrt{3}} \cdot \sqrt{(R_s \cdot i_{sx} - \omega \cdot \psi_{sy})^2 + (R_s \cdot i_{sy} + \omega \cdot \psi_{sx})^2} \tag{2.13}$$

$$\psi_s = \frac{u_{batt}}{\omega_{el} \cdot \sqrt{2}} \tag{2.14}$$

$$\omega_{el} = \omega_{mech} \cdot \frac{P}{2} \tag{2.15}$$

2.7 Drive cycle

Since these simulations are made for a new type of vehicle with new applications, no existing drive cycles can be used. Instead, existing cycles are modified to reflect the anticipated usage patterns of this specific vehicle. These modifications involve scaling the cycles to match the vehicle's top speed and acceleration capabilities, ensuring an accurate representation of the vehicle's performance. Since the vehicle is likely to be used in shorter durations than those for which these drive cycles are originally designed, the timescales are also adjusted.

This study focuses on the use of the LEVKART in industrial applications. In these scenarios, the vehicle will likely be used with an inconsistent speed profile, some stoppage time, and where high acceleration is crucial. Therefore, a drive cycle that represents city driving conditions might be an accurate representation after some modifications. Figure 2.7 shows the EPA Urban Dynamometer Driving Schedule (UDDS) that represents city driving conditions [11]. The y-axis on this cycle represents the velocity, expressed in *m/s*. As can be seen in the figure, the top speed according to this driving schedule is 25 m/s, which is approximately 90 km/h. The top speed for the LEVKART is 35 km/h, which is why this drive cycle needs to be scaled down.

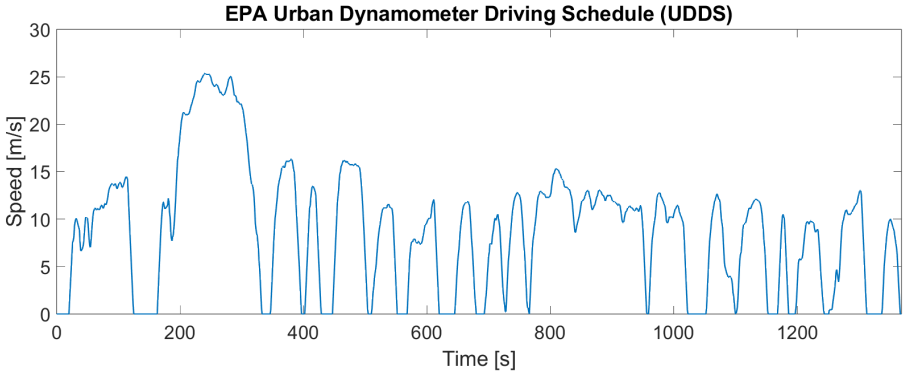

Figure 2.7: EPA Urban Dynamometer Driving Schedule (UDDS)

Figure 2.8 shows the UDDS after the modifications. The y-axis in this figure represents the velocity in m/s, and the x-axis represents time in seconds. As can be seen in the figures, both the x- and y-axis are scaled down to better represent the behavior of the LEVKART. The maximum speed is reduced from 90 km/h (25 m/s) to 35 km/h (10 m/s). The timescale is adjusted from 1369 seconds to 550 seconds to ensure a realistic acceleration for the new drive cycle. The speed is reduced by 40%, and the timescale is therefore also reduced by the same percentage.

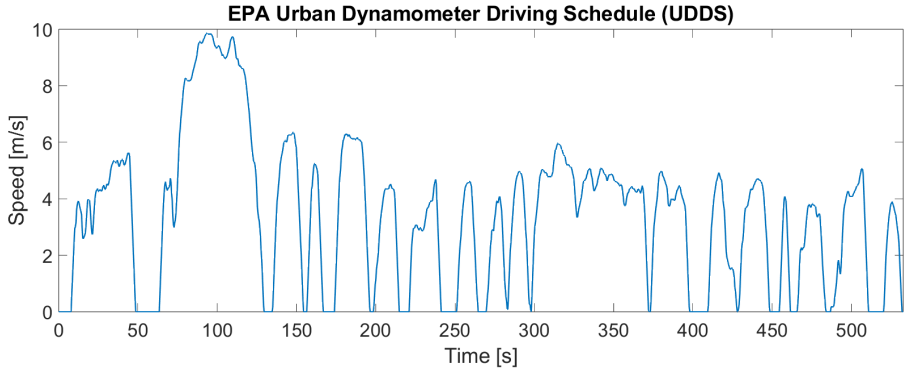

Figure 2.8: Modified version of the EPA Urban Dynamometer Driving Schedule (UDDS)

Another drive cycle that is also implemented and modified to use as a comparison is the EPA FTP Highway Motorcycle Driving Schedule, which can be seen in figure 2.9. This cycle represents the driving behavior of a motorcycle with a maximum speed of approximately 60 km/h, or 17 m/s [11].

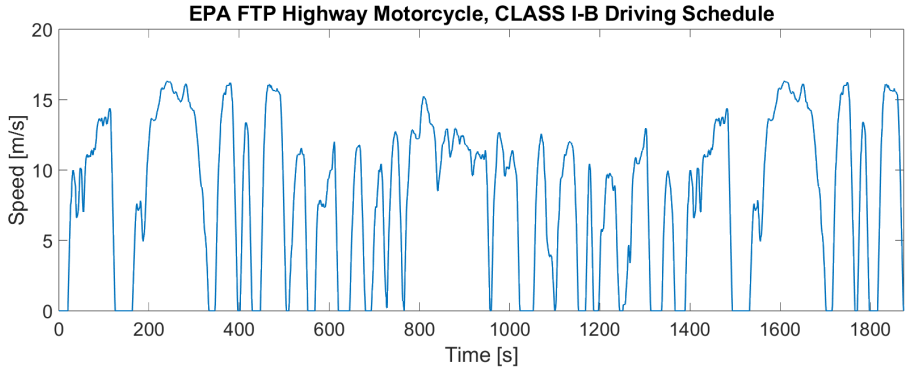

Figure 2.9: EPA FTP Highway Motorcycle, CLASS I-B Driving Schedule

Figure 2.10 shows the drive cycle after the modifications. This cycle originally had a top speed of around 60 km/h and is scaled down to have a top speed of 35 km/h (or 10 m/s). Following the same methodology as the previous drive cycle, the time at the x-axis is scaled down to match the new top speed. What was originally a timescale of 1874 seconds is reduced to 1117 seconds, which can be seen in the figures.

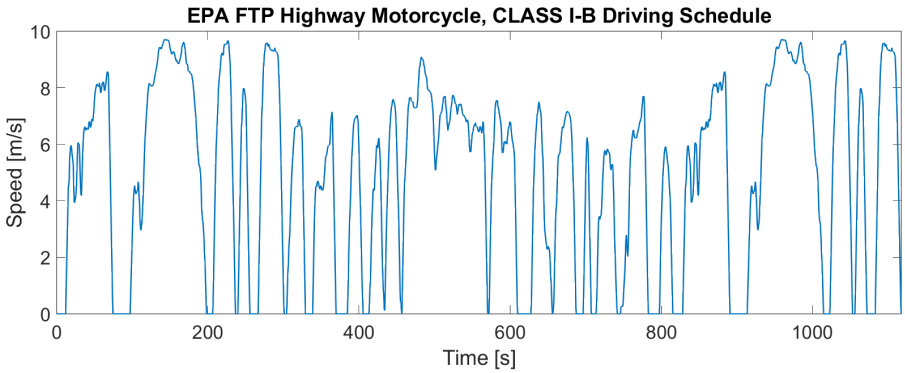

Figure 2.10: Modified version of the EPA FTP Highway Motorcycle, CLASS I-B Driving Schedule

These adapted cycles serve as an approximation of the vehicle's behavior during industrial use, assuming that the vehicle would be used in applications where high acceleration and high speeds are necessary. Should the vehicle's application extend to urban environments, new cycles would have to be created. These cycles would use a lower top speed of 20-25 km/h and have a more consistent velocity profile with less stoppage time and less acceleration and deceleration.

2.8 Model Validation and Calibration

One simple method to assess the accuracy of the simulation model is to compare the simulation results to a real-world test with the prototype vehicle. Ideally, such comparisons should be performed on all subsystems to evaluate their accuracy. However, due to practical limitations, this was only conducted on the overall system, serving as an indication of how accurately the simulation model represents the actual vehicle by comparing the measured range with the simulated range. However, if the actual range does not correspond to the simulated range, it can depend on several factors and it would be hard to determine which one is at fault. It could be any of the equations in the model, any parameters that are estimated, or another factor that is not accounted for.

The test cycle is performed when the vehicle is fully charged, and it is driven until the battery is fully depleted to obtain the vehicle's range. The driving behavior during the tests mimics real-world usage, following the anticipated driving patterns of the intended application. The vehicle speed is logged during the test. This data is converted to a drive cycle in the same format as those discussed in section 2.7, and the drive cycle is inserted in the simulation model. The range of the vehicle is simulated in the Simulink model and compared to the measured range. The accuracy of this measured test cycle is further discussed in section 5.1.

2.9 Assumptions

Certain assumptions about the vehicle parameters are necessary in developing the simulation model for this vehicle, particularly due to external factors influencing the vehicle's performance. Given the vehicle's relatively small size, the driver's weight and the load constitute a substantial proportion of the total weight, which affects the vehicle's performance and energy consumption. Similarly, the frontal area and the drag coefficient vary based on the driver and the load. Given the vehicle's size and its energy requirements for auxiliary components, the auxiliary power is negligible and is set to zero in this simulation model.

Various loads are tested to ensure that the vehicle will function as intended when carrying the desired maximum load. However, the total weight is set to 100 kg in the initial simulations. This includes the driver, potential loads, and the vehicle itself. The rolling resistance is estimated since this data is not available for the tires that are currently being used in the LEVKART, and is assumed to be $C_r = 0.02$. The frontal area is set to $Av = 0.6$, which is an estimation for an average adult in a standing position. The drag coefficient for an average adult is around 1.0-1.3 [12]. This is set to 1.1 in the initial simulations.

2.10 Simulations

Once the Simulink model is complete and gives an accurate representation of the vehicle, the parameters are varied to examine how the vehicle behaves with different settings. The main focus is to evaluate different batteries and configurations of battery cells. Which battery voltage is most favorable for the LEVKART? What capacity should the battery have to achieve a desirable range for the vehicle?

Since the measured data of the current electric machine is inputted into the model, the machine can not be changed without performing new tests. The power rating can be evaluated and the simulations can help determine if the machine is of sufficient size and power. However, if a new machine were to be simulated, new measurements would have to be performed to provide representative values of the new machine.

The same applies to the power electronic components. Since they have parameters that are specific to the components that are currently being used in the vehicle, these parameters would also have to be changed if new components were to be simulated and tested. This process would be less time-consuming than for the electric machine, as these parameters could be retrieved from the manufacturer's datasheet instead of being measured through tests. However, the main focus is on simulating the vehicle's performance with different batteries, using the same machine and power electronic components that are being used today.

The simulation model outputs estimated energy consumption and the corresponding range, the driving distance of a full charge. Graphs about how well the vehicle followed the drive cycle are also presented. This helps determine if the simulated powertrain configuration with specific parameters can perform as desired. Based on this data, different batteries are simulated to find the optimal solution and how the vehicle's powertrain should be configured to reach the highest range while still adhering to the specific constraints and requirements regarding the vehicle.

3 Electric Machine Testing

This chapter aims to provide an insight into the methodology and the procedure of the testing phase. The chapter describes the equipment, how the tests are performed, and what data is collected.

3.1 Overview

The goal of the simulations is not only to suggest the optimal powertrain configuration for different scenarios and applications but also to give a realistic estimation of the range of the vehicle with these different battery packs. To ensure this, the simulation model must reflect the actual vehicle as accurately as possible. For this reason, the electric traction machine currently used in the prototype vehicle is tested to gather certain parameters needed to obtain an accurate representation of the machine in the Simulink model. A test setup is designed specifically for this machine, and the parameters that are measured from the tests are integrated into the simulation model. This ensures that the simulation model is as accurate as possible, allowing comparison between the model and the actual vehicle. If the simulated range and driving behavior do not match the real vehicle, the simulation model would have to be modified and corrected.

These measured parameters allow for an estimation of the expected range during different drive cycles and powertrain configurations. It also allows for an accurate evaluation of the size of the machine. Parameters related to the driver and the load can be adjusted to evaluate if the selected machine is of appropriate size. If the vehicle fails to achieve the desired top speed and acceleration with the maximum load, it may be necessary to consider a machine with a higher power. The same applies for the opposite scenario. If the vehicle reaches the maximum speed and acceleration with the maximum load without any problems, different machines with a lower power rating can be simulated, as they might be sufficient for the specific application.

3.1.1 Electric Machine Type

The choice of machine type is critical in the development of powertrains for light electric vehicles due to their direct impact on the vehicle's overall efficiency. The machine currently used in the vehicle is a Permanent Magnet Synchronous Motor (PMSM) hub motor, which is directly integrated into the wheel [13]. This specific machine can be seen in figure 3.1. The compactness of the hub motor is beneficial for an electric vehicle of this size with limited space. PMSMs are particularly advantageous due to their high efficiency and minimal energy losses during operation. These machines utilize permanent magnets which produce a consistent magnetic field, thereby reducing the electrical losses typically associated with other machine types. The lower energy consumption of PMSMs enhances not only the vehicle's performance but also contributes to a longer range, making them ideal for urban mobility solutions [14].

Figure 3.1: The PMSM hub motor used in the LEVKART

Table 3.1 shows some key specifications for the PMSM hub motor used in the LEVKART. These values are either retrieved from the manufacturer's website [13], or estimated based on measurements from the actual machine. The LEVKART uses two of these PMSM hub motors, one in each front wheel. However, in the simulation model, these machines are represented by a single machine with double the power output.

Specification	**Value**	**Specification**	**Value**
Motor Case Diameter	165 mm	Motor Max Power	2000 W
Motor Width	55 mm	Number of Poles	40
Motor Weight	1776 g	Max Torque	12 Nm
Stator Weight	924 g	Max Efficiency	89%
Rated Power	1200 W	Resistance (25°C)	134 Ω

Table 3.1: Specifications for the machine used in the LEVKART

3.2 Test Setup

During the tests, the electric machine is physically connected to the test rig with a horizontal axle. For this purpose, a custom part is designed and manufactured that is attached to the side of the electric machine. Figure 3.2 shows a model of the manufactured part. With this part connecting the machine to the test rig, the machine can be run at different speeds while braking at various torque levels from the rig to gather all necessary data. This process is further described in section 3.3.

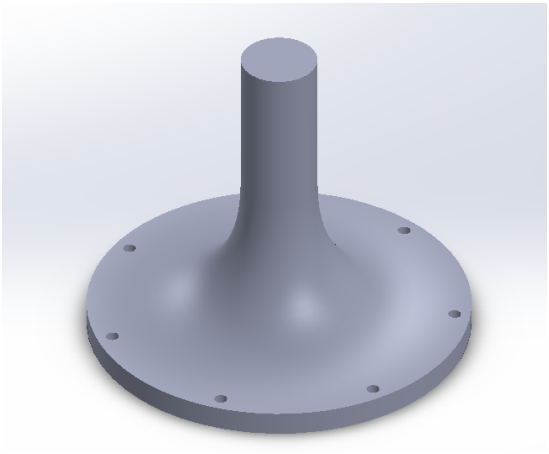

Figure 3.2: Custom part that was manufactured for the tests

Figure 3.3a shows the manufactured axle mounted to the hub motor. The machine with the attached axle is connected to the rest of the test rig as can be seen in figure 3.3b. The rig consists of a DC machine that is operated through a separate computer, while the PMSM hub motor is connected and operated through a software called VESC Tool.

(a) The finished part mounted to the hub motor

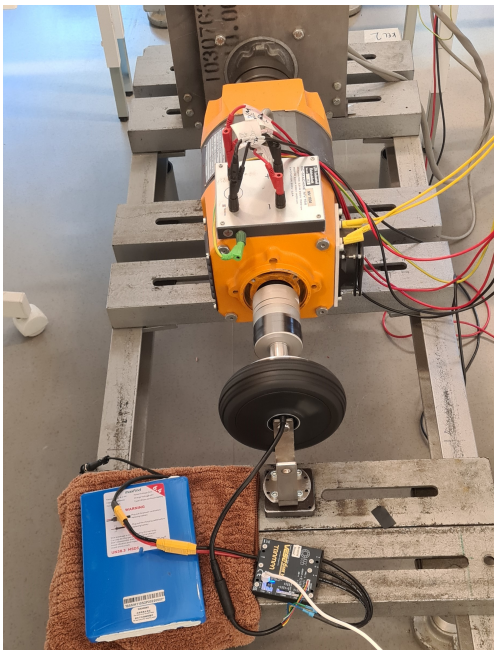

(b) The complete test setup, with the machine connected to the test rig

Figure 3.3: Test rig setup

3.2.1 Motor Controller

To control and monitor the performance of the PMSM during the testing process, a motor controller called VESC is used [15]. The VESC controller is a highly flexible and open-source solution, which is managed through the VESC Tool software. This software allows real-time data monitoring and adjustment of key machine parameters, such as speed, current, and voltage, which are essential in evaluating the machine's performance.

Additionally, the VESC Tool allows for real-time monitoring of direct axis and quadrature axis currents and voltages, providing valuable insight into the machine's behavior under different speeds and loads. The software stores all parameters in a CSV file for post-analysis. These features make the VESC controller an effective tool for both controlling and evaluating the PMSM machine comprehensively.

3.3 Test Procedure

A series of tests are performed with the PMSM physically connected to the DC machine (the orange machine in figure 3.3b) acting as a load, enabling control over the torque applied to the PMSM. A range of torque levels are applied through the DC machine, while the PMSM machine is operated at varying speeds for each torque level. Data is collected at each torque and speed combination through the VESC Tool software.

Testing begins with the PMSM operating at 1000 ERPM, which is the electric RPM that is converted to mechanical RPM by dividing by the number of pole pairs, with an applied torque of 1 Nm. Using the VESC Tool, the speed of the PMSM is gradually increased with steps of 500 ERPM until it reaches a maximum speed of 13000 ERPM (650 mechanical RPM), which is determined to be the maximum speed the machine can safely operate at. The applied torque is increased to 2 Nm, and the procedure is repeated. This process continues, with the applied torque increasing incrementally until it reaches 4 Nm, at which point the PMSM machine only manages to achieve a speed of 9500 ERPM. The measurements proceed with an applied torque of 5 Nm, where the PMSM reaches a speed of 6000 ERPM. The test is concluded at this stage, as the machine could not withstand an applied torque of 6 Nm. Some of the key parameters gathered during the tests can be seen in Appendix B.4.

To ensure the accuracy of the speed readings provided by the VESC Tool, the actual speed of the PMSM machine is independently measured using a laser tachometer, as can be seen in figure 3.4, and compared to the VESC Tool speed readings.

Figure 3.4: Measurments of the RPM of the PMSM machine

3.4 Data Collection

The equations in section 2.5 highlight the necessity of specific parameters regarding the machine to accurately represent the losses. These parameters include the currents i_{sx} and i_{sy}, the flux linkages ψ_{sx} and ψ_{sy} and the torque T. The estimation of these parameters is therefore the focal point of the tests. The currents i_{sx} and i_{sy} are read directly from the software, whereas the flux linkages and the torque measurements involve more complex methodologies, and need to be calculated using the equations in sections 3.4.1 and 3.4.2. The resulting data from the tests are presented as a range of parameters in a CSV file, with the focus on extracting i_{sx}, i_{sy}, u_{sx}, u_{sy} and ERPM.

The tests yield over 16000 measurement points, with approximately 160 measurement points for each speed and corresponding torque level. The parameters needed are measured or calculated at each measurement point and averaged for each RPM level, compensating for any deviations in the measurement.

3.4.1 Torque

The generated torque from the electric machine can not be measured directly with the equipment and software that are being used during the tests. Instead, it is calculated using equation 3.1. P_{loss} in this equation is an estimation of the iron losses from the stator in the machine. This estimation is based on [16], which serves as an approximation of the losses in W/kg. The weight of the stator is an estimation based on measurements of its volume and by assuming its density, resulting in a stator weight of 0.924 kg. The iron losses corresponding to equation 2.10, vary with frequency, with specific values provided for 50, 100, 200, and 400 Hz [16], corresponding to 3000, 6000, 12000, and 24000 ERPM. These values are interpolated to determine the corresponding P_{loss} for each measurement point. Subsequently, these interpolated values are averaged to obtain a single P_{loss} value for each RPM and corresponding torque level. For this machine, the estimated iron losses are 0.91 W, 1.98 W, 5.67 W, and 15.80 W, respectively, at 50 Hz, 100 Hz, 200 Hz, and 400 Hz.

The remaining parameters in the equation are retrieved from the controller during the tests, where ω_{mech} is the electrical RPM divided by the number of pole pairs and converted to angular velocity in *rad/s*. R_s is the stator resistance which is obtained from a datasheet for the machine from its manufacturer [13].

$$T = \frac{(u_{sx} - R_s * i_{sx}) * i_{sx} + (u_{sy} - R_s * i_{sy}) * i_{sy} - P_{loss}}{\omega_{mech}} \tag{3.1}$$

3.4.2 Flux linkage

The flux linkages ψ_{sx} and ψ_{sy} can not be directly measured, but needs to be calculated using the equations below.

$$u_{sx} = R_s \cdot i_{sx} + \frac{d}{dt}(\psi_m + L_{sx} \cdot i_{sx}) - \omega_r \cdot L_{sy} \cdot i_{sy} \tag{3.2}$$

$$u_{sy} = R_s \cdot i_{sy} + L_{sy} \cdot \frac{di_{sy}}{dt} + \omega_r \cdot (\psi_m + L_{sx} \cdot i_{sx}) \tag{3.3}$$

$$\psi_{sx} = \psi_m + L_{sx} \cdot i_{sx} \tag{3.4}$$

$$\psi_{sy} = L_{sy} \cdot i_{sy} \tag{3.5}$$

R_s in equations 3.2 and 3.3 is the stator resistance, which can be found in the manufacturer's datasheet. For this specific machine, it is $R_s = 134m\Omega$. The second term in both equations is assumed to be negligible since there are no fluctuations in magnetic flux and the rate of change (i.e. the derivatives) could effectively be zero. Equations 3.4 and 3.5 are the flux relations [4]. By combining these relations with equations 3.2 and 3.3, equations 3.6 and 3.7 are derived. These equations express the flux linkages ψ_{sx} and ψ_{sy} in terms of the voltages u_{sx} and u_{sy}, the currents i_{sx} and i_{sy}, the stator resistance R_s and the rotors electrical angular velocity ω_r. All of these parameters are either known or can be measured during the tests, which allows for the calculation of the flux linkages. Some of the parameters that are measured or calculated from the tests can be seen in Appendix B.4.

$$\psi_{sx} = \frac{u_{sy} - R_s \cdot i_{sy}}{\omega_r} \tag{3.6}$$

$$\psi_{sy} = \frac{R_s \cdot i_{sx} - u_{sx}}{\omega_r} \tag{3.7}$$

4 Results

This chapter presents the results of the simulations with regard to the goals specified in section 1.2.

4.1 Overview

The focal point of this project is to investigate the vehicle's performance with different battery voltages to determine the optimal battery pack for the specified applications. With the optimal battery pack determined, other parameters, such as the rated power of the electric machine and other parameters regarding the power electronic components, may be modified to examine if the energy consumption can be reduced further without compromising the vehicle's performance. Alternative machines might be considered if the simulations indicate that the rated power of the current machine is either insufficient or unnecessarily high.

To verify that the simulation model is able to fulfill the performance requirements under several scenarios, both drive cycles presented in section 2.7 are used and compared. These drive cycles are both applicable for industrial use cases but have a varied velocity profile, which allows for comparison of the results. The drive cycle presented in figure 2.8 which is a modified version of the EPA Urban Dynamometer Driving Schedule, is referred to as Drive Cycle 1 when presenting the results. The second drive cycle, which is a modified version of the EPA FTP Highway Motorcycle driving cycle that is presented in figure 2.10, is referred to as Drive Cycle 2 when presenting the results. The simulations are performed with the initial parameters specified in section 2.9.

4.2 Drive Cycle 1

Table 4.1 shows the resulting energy consumption and range with different battery voltages when running the simulations with drive cycle 1. The SoC represents the drop in state of charge, starting at 90% for all three batteries. The graphs for the SoC is presented in Appendix B.

Battery Voltage	**Energy Consumption** ($\frac{kWh}{10km}$)	**Capacity** (Wh)	**Range** (km)	**SoC** (%)
36 V	0.146	418	28.6	83.2
39.6 V	0.129	345	26.7	82.7
43.2 V	0.133	376	28.3	83.1

Table 4.1: Range and energy consumption for different battery voltages with drive cycle 1

Figure 4.1 illustrates the vehicle's performance throughout drive cycle 1. The yellow line represents the reference speed and the blue line shows how closely the vehicle is able to follow this desired velocity profile. This particular simulation is conducted using the 43.2 V battery pack. As can be seen from the figure, the vehicle successfully follows the drive cycle and is able to reach both the maximum speed and the desired acceleration with this configuration. This indicates that the vehicle's powertrain is capable of meeting the performance demands of this drive cycle.

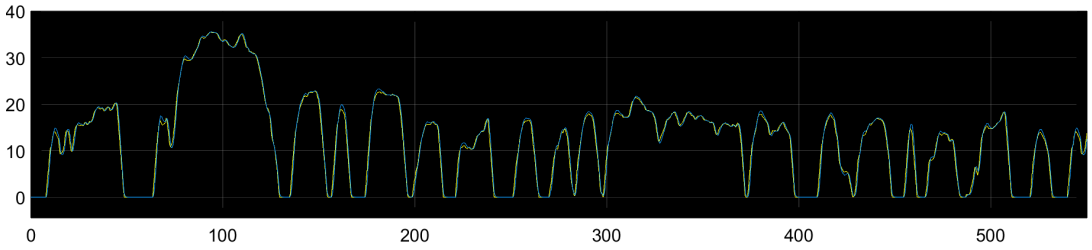

Figure 4.1: Simulation of drive cycle 1, speed[km/h] time[s], with the 43.2 V battery pack

4.3 Drive Cycle 2

The same procedure is performed for the second drive cycle. Table 4.2 shows the resulting energy consumption and range for different battery voltages.

Battery Voltage	**Energy Consumption** ($\frac{kWh}{10km}$)	**Capacity** (Wh)	**Range** (km)	**SoC** ($\%$)
36 V	0.131	418	31.9	72.3
39.6 V	0.111	345	31.1	72.0
43.2 V	0.118	376	31.9	72.3

Table 4.2: Range and energy consumption for different battery voltages with drive cycle 2

Figure 4.2 shows the vehicle's behavior during drive cycle 2, which is also simulated with the 43.2 V battery pack. As with the previous simulation, the LEVKART effectively follows the desired velocity profile and reaches the specified maximum speed.

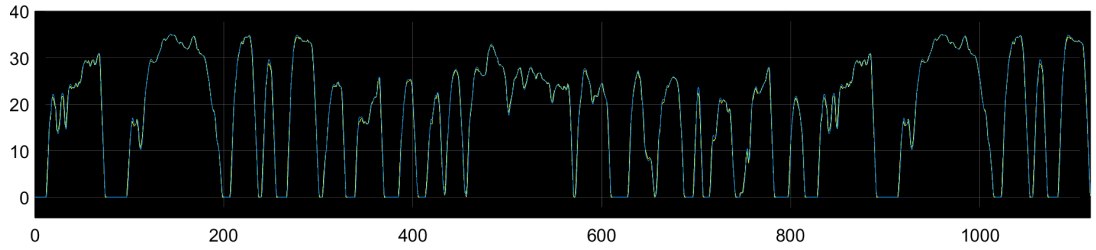

Figure 4.2: Simulation of drive cycle 2, speed [km/h] time [s], with the 43.2 V battery pack

5 Discussion

This chapter discusses the results and what insights they led to, as well as which parts could still use some improvements in future work.

5.1 Model Validation

The methodology for assessing the accuracy of the overall system by comparing the simulated range to the measured range, as discussed in section 2.8, proved to be somewhat problematic. Figure 5.1 shows the drive cycle from the range tests, with the yellow line representing the actual speed (km/h) of the LEVKART during the tests, and the blue line shows the simulation model's attempt to follow this cycle. The time on the x-axis is given in seconds.

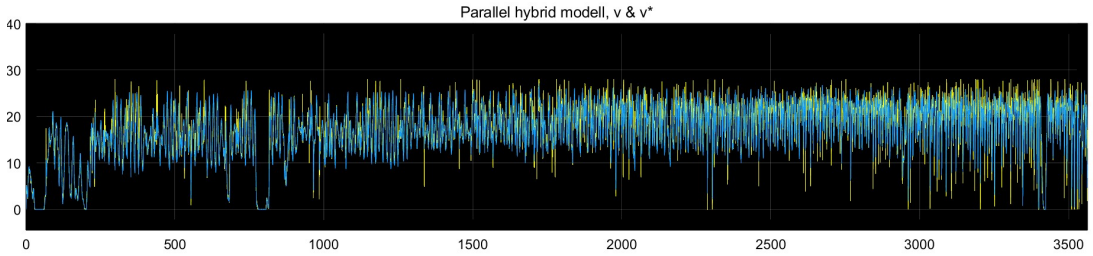

Figure 5.1: Cycle from the range measurements

The simulation model struggles to follow this cycle that is obtained from the range test, especially at the high-speed parts with high accelerations. Figure 5.2 shows a zoomed-in section of the cycle that shows how the simulation model fails to track the small variations in speed from the test cycle. The motor accelerations that the graphs present are not realistic for this vehicle. This is most likely due to wheelspin. The speed of the vehicle is measured by the speed of the wheels, and not the actual speed of the vehicle. This means that any wheelspin could cause anomalies in the cycle, leading to inaccurate vehicle acceleration and deceleration data in the simulation.

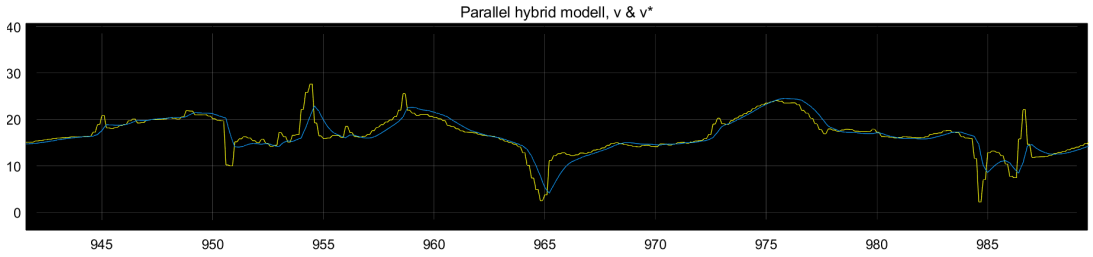

Figure 5.2: A section of the cycle from the range measurements

Despite the limitations of the cycle for use with the simulation model, it provides valuable information about the vehicle's range. The tests show that the vehicle is capable of driving 17.2 km with one charge. This value can be used as a reference point when running simulations with other cycles and comparing their range. This is not a perfectly accurate method of validating the model, but it gives an insight into whether the simulated range is realistic or not since the other cycles follow a similar pattern as the one in figure 5.1, a varied speed profile with high accelerations and decelerations.

5.1.1 Simulated Range

When the range of the actual vehicle is tested, as discussed in section 2.8, a 43.2 V battery is used. If the model is accurate, even if the drive cycles are not very similar, the simulated range for the 43.2 V battery, as presented in tables 4.1 and 4.2, should at least come close to the measured range of the vehicle, which is 17.2 km. When using Drive Cycle 1, the range is simulated to be 28.3 km, and when using Drive Cycle 2, the range is simulated to be 31.9 km. Since these drive cycles differ significantly from the test cycle shown in figure 5.1, a more accurate estimation of the simulated range might be obtained by averaging the results from these two drive cycles. This resulted in a simulated range of 30.1 km with the 43.2 V battery.

This difference between the simulated range and the measured range could be due to a variety of factors. It is possible that some of the vehicle parameters are inaccurately assumed, or that certain losses were not fully accounted for in the simulation. Additionally, the significant difference between the test cycle and the simulated drive cycles likely contributes to this variation. The averaged values between the two drive cycles with the different battery voltages are presented in table 5.1.

Battery Voltage	**Energy Consumption** ($\frac{kWh}{10km}$)	**Capacity** (Wh)	**Range** (km)
36 V	0.139	418	30.3
39.6 V	0.120	345	28.9
43.2 V	0.125	376	30.1

Table 5.1: Average range and energy consumption between the two drive cycles

5.2 Result

The results presented in table 5.1 show that the energy consumption decreased slightly when reducing the battery voltage from 43.2 V to 39.6 V. The 39.6 V battery also had a lower energy content of 345 Wh, which led to a 4% reduction in the overall range. However, when switching to the 36 V battery with a 10s4p cell configuration, the energy consumption increased. This battery had a higher energy content of 418 Wh, leading to an overall range that is roughly the same as the 43.2 V battery.

As shown in the comparison in table 5.1, particularly when comparing the 39.6 V battery to the 36 V battery, the energy consumption does not always decrease when lowering the voltage. This indicates that other factors, such as battery configuration and system losses, play a significant role in performance. Therefore, it is crucial to balance battery voltage, energy content, and energy consumption when designing battery systems for optimal performance.

Figures 5.3, 5.4, and 5.5 illustrate the different cumulative losses during the simulations with Drive Cycle 1, expressed in Wh. The green line in each graph corresponds to the 36 V battery, the red line to the 39.6 V battery, and the blue line to the 43.2 V battery. Figure 5.3 shows the losses from the battery subsystem in the Simulink model.

Even though the 36 V battery has the lowest internal resistance, the graph shows that it has higher losses than the 39.6 V and the 43.2 V batteries. This indicates that other factors are influencing the battery's performance in the simulation model. The issue likely lies in where the efficiency is being calculated within the battery subsystem. The way the model calculates the power output may not accurately reflect real-world behavior, especially when switching cell configurations, and may require further refinements to ensure realistic battery efficiency.

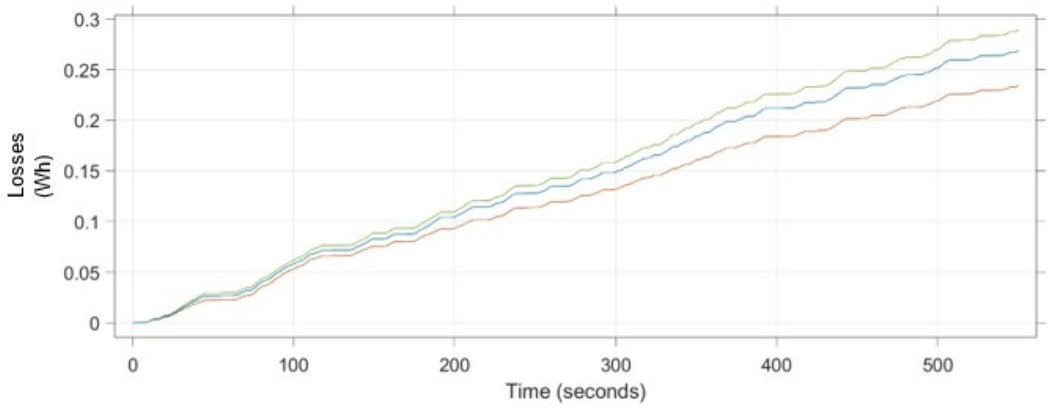

Figure 5.3: Battery losses, green - 36 V, red - 39.6 V, blue - 43.2 V

Figure 5.4 illustrates the losses in the power electronics subsystem, where the 36 V battery again has the highest losses, followed by the 39.6 V battery, and the 43.2 V battery with the lowest losses. Figure 5.5 shows the losses in the subsystem for the electric machine, where all three batteries display nearly identical performance. This suggests that the machine's efficiency is relatively consistent across the different battery voltages.

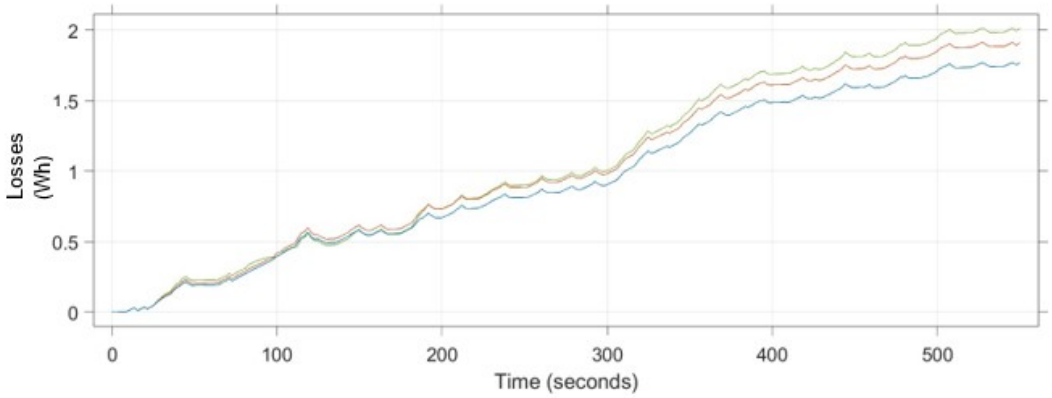

Figure 5.4: Power electronics losses, green - 36 V, red - 39.6 V, blue - 43.2 V

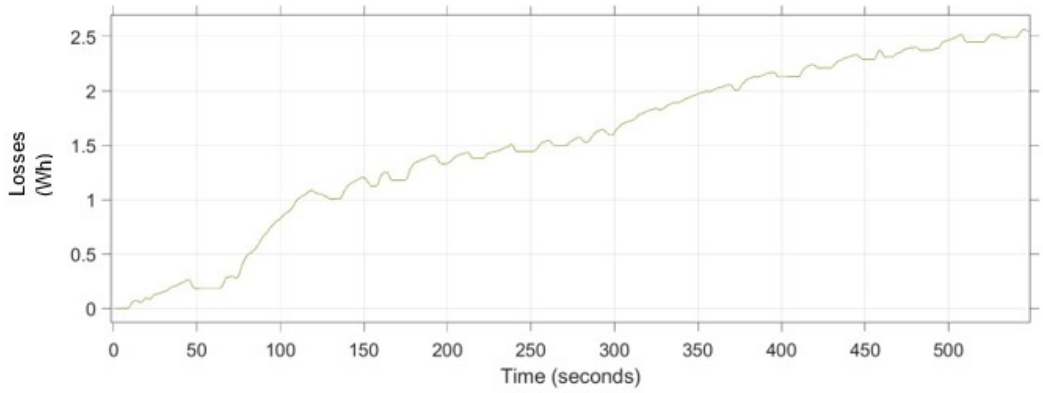

Figure 5.5: Electric machine losses, green - 36 V, red - 39.6 V, blue - 43.2 V

5.3 Further Research

While the model provides some valuable insights, it is clear that further development is necessary before it can fully and accurately represent the vehicle's behavior across various scenarios and be considered completely reliable. The primary concern is the discrepancy between the measured range and the simulated range. Even though the drive cycles differ significantly from the test cycle that was logged during the range test, the simulated range should at least come close to the measured range. This difference indicates that the Simulink model is not yet fully reliable and would benefit from additional refinements before being able to provide more realistic estimations of the LEVKART's range.

5.3.1 Drive Cycles

One area that could benefit from some improvements is the drive cycles. These are estimations of how the vehicle would be used in real-world conditions. As more data is gathered from actual usage, it would be possible to create more accurate drive cycles. Particularly, the cycle developed during the range testing of the vehicle could use some refinements. As discussed in section 5.1, the vehicle's speed is measured by the speed of the wheels rather than the actual speed of the vehicle. Although this cycle provided an estimation of the range of the vehicle, it would have been more valuable if the actual vehicle speed had been logged. This would have provided a more reliable means of assessing the model's overall performance, ensuring that the simulated range matches the measured range if this cycle could have been followed more precisely.

5.3.2 Electric Machine and Power Electronic Components

The model only compares different battery packs and does not compare different electric machines or power electronics components. Data are retrieved for the components currently used in the vehicle, and the electric machine is tested to gather all relevant data. While machines with different power ratings could be compared, a more thorough comparison would require testing the different machines in the same manner as in the original tests. This could involve manufacturing new components for the test rig, as the existing ones might not fit other machines. Similarly, if new power electronic components are considered, data would have to be gathered and integrated into the model to fully assess their impact on the vehicle's performance. However, the simulation model can help assess whether the current machine is appropriately sized by varying the power output and predicting performance outcomes, but an accurate assessment of a new machine would ultimately require further tests.

5.3.3 Model Assumptions and Limitations

The current simulations are conducted with several limitations and assumptions, particularly related to the vehicle, the driver, and the environment in which the vehicle operates. One of these assumptions about the vehicle is the rolling resistance coefficient C_r, which is set to 0.02. This value is a rough estimation since this data is not available for the specific tires used in the LEVKART, and might not be perfectly accurate. Other assumptions include the frontal area of the vehicle and driver A_v, and the drag coefficient C_d. These are estimated to $A_v = 0.6$ and $C_d = 1.1$. While these values are reasonable estimates, they could benefit from further exploration and more precise measurements or calculations, potentially for different drivers to better represent a range of scenarios.

5.4 Conclusion

The results indicate that while the simulation model provides valuable insights regarding the comparison between different battery voltages, further refinements are needed for it to be fully reliable. Despite the discrepancy between the measured and simulated range, the comparison between the three battery packs can still be considered meaningful, even if the values for the simulated range might not reflect real-world performance.

The simulation results for the different batteries suggest that switching to a 39.6 V battery (11s3p - 345 Wh) using the same type of cells, would likely reduce the range of the vehicle, making this a less favorable option. Switching to a 36 V battery (10s4p - 418 Wh) with the specifications detailed in section 2.3, would result in a range similar to the 43.2 V battery (12s3p - 376 Wh) according to these simulations. Although the 36 V battery has a higher energy consumption, its larger energy content compensates, resulting in a similar range.

In conclusion, while the model would benefit from further work to improve its accuracy, it still provides useful guidance on which battery pack might be most suitable for the LEVKART during the specified use cases. Based on the simulations, there appears to be no significant advantage in switching from the current 43.2 V battery to one of the other options, as these would result in either a shorter or a similar range.

Bibliography

[1] European Parliament. *Fit for 55: Zero CO2 emissions for New Cars and vans in 2035: News: European parliament*. URL: https://www.europarl.europa.eu/news/en/press-room/20230210IPR74715/fit-for-55-zero-co2-emissions-for-new-cars-and-vans-in-2035.

[2] Future Market Insights. *Electric Scooters Market Analysis*. 2023. URL: https://www.futuremarketinsights.com/reports/electric-scooters-market.

[3] Nordic Micro Mobility Association. *Remissvar till Statens väg- och transportforskningsinstituts (VTI) utredning*. 2022. URL: path_to_pdf/nordic-micromobility-association.pdf.

[4] Mats Alaküla and Per Karlsson. *Power Electronics: Devices, Converters, Control and Applications*. Tech. rep. Department of Industrial Electrical Engineering and Automation, Lund University, 2014.

[5] Inès JORGE, Tedjani MESBAHI, Théophile PAUL and Ahmed SAMET. "Study and simulation of an electric scooter based on a dynamic modelling approach". In: *2020 Fifteenth International Conference on Ecological Vehicles and Renewable Energies (EVER)*. 2020.

[6] Olaf Korzilius, Olaf Borsboom, Theo Hofman and Mauro Salazar. "Optimal Design of Electric Micromobility Vehicles". In: *2021 IEEE International Intelligent Transportation Systems Conference (ITSC)*. 2021.

[7] *Test of Samsung INR18650-29E 2900mAh*. URL: https://lygte-info.dk/review/batteries2012/Samsung%20INR18650-29E%202900mAh%20%28Blue%29%20UK.html.

[8] *Maxfind Battery*. URL: https://www.maxfind.com/products/battery?variant=39577197936705.

[9] Ilyès Miri, Abbas Fotouhi and Nathan Ewin. "Electric vehicle energy consumption modelling and estimation—A case study". In: *International Journal of Energy Research* (2021). DOI: https://doi.org/10.1002/er.5700.

[10] Infineon. *IRF7749L1TRPbF Product Datasheet*. 2019. URL: https://www.infineon.com/dgdl/irf7749l1pbf.pdf?fileId=5546d462533600a4015356043d6b1ca0.

[11] *EPA Urban Dynamometer Driving Schedule*. URL: https://www.epa.gov/vehicle-and-fuel-emissions-testing/dynamometer-drive-schedules.

[12] Abdulkareem Sh Al-Obaidi and Mun Koo. "Calculation of Aerodynamic Drag of Human Being in Various Positions". In: 2013.

[13] *Maxfind Hub Motors*. URL: https://www.maxfind.com/products/hub-motor?variant=32105170468929.

[14] Nilay Awasthi. "Designing of Electric Vehicle Using MATLAB and Simulink". In: *Proceedings of the International Conference on Recent Advances in Computational Techniques (IC-RACT)*. 2020.

[15] Trampaboards. *VESC MkVI*. 2024. URL: https://trampaboards.com/vesc-6-mkvi--trampa-gives-you-maximum-power-p-34848.html.

[16] Tata Steel in Europe. *Typical data for SURA® M250-35A*. 2008. URL: https://www.tatasteeleurope.com/sites/default/files/m250-35a.pdf.

Appendix A

Matlab Code and Simulink Model

This appendix presents the Simulink model and parts of the Matlab code that were used. The entirety of the original model that this study was based on is not included, but only selected parts from the code that were modified to be applicable for the LEVKART

A.1 Matlab Code

```
case 6 %LEVKART
    Wbatt = 0.376*3.6e6;    % [Ws]
    Mv = 100;          % Vehicle weight [kg], LEVKART weight - 18kg
    rw = 0.165/2;           % wheel radius (m)
    Cd = 1.1;             % air_resistance
    Cr = 0.01;            % roll resistance
    Av = 0.5;    % Front area [m2]
    vmax = 35/3.6;       % Top speed [m/s]
    Pem_max = 2000;    % Traction machine power [W]
    Number_of_gears = 1;
    Paux = 0;           % Without AC, assumed
end
```

Listing A.1: Parameter Initialization for LEVKART

```
Vnom = 48;
Inom_cell = 2.9;
Inom = 3 * Inom_cell;
I_peak = 3 * 8.25;
I_max = 3 * 5.5;
Pbatt_max = Vnom * Inom;

[EtaBATT,Pbatt,Mbatt,Pbatt_max_new,Wbatt_new]=CreateBATTmap(
    ↪ Pbatt_max,Wbatt,Vnom);
SOC_batt_start_value = 90; % Start value of SOC
SOC_tract_min = 10;
SOC_tract_max = 90;

% Based on Samsung cell data from https://lygte-info.dk/review/
    ↪ batteries2012/Samsung%20INR18650-29E%202900mAh%20%28Blue
    ↪ %29%20UK.html
% for a case with 0.2 A discharge current

Ubatt = 43.2;
Wbatt = 0.376*1000*3600; % 0.2 kWh i Ws

% Calculate battery characteristics at Cell level
load SamsungCell1.mat
Wbatt_cell_nom = 10.609*3600; % Ws
Wbatt_cell = zeros(length(SamsungCell1(:,1)));
Wbatt_cell(1) = Wbatt_cell_nom;
Ubatt_cell_nom = 3.65; % V
Ibatt_cell_max = 2.75;  % A
SOC(1) = 100; % %
Rbatt_cell = 0.06;  % Ohm

e_batt_cell(1) = Rbatt_cell*0.2 + SamsungCell1(1,2);

for i=2:length(SamsungCell1(:,1))
    e_batt_cell(i) = Rbatt_cell*0.2 + SamsungCell1(i,2);
    Wbatt_cell(i) = Wbatt_cell(i-1) - (SamsungCell1(i,1)-
    ↪ SamsungCell1(i-1,1))*3600*SamsungCell1(i,2);
    SOC(i) = Wbatt_cell(i)/Wbatt_cell_nom*100;
end
figure(4), clf
subplot(1,2,1)
plot(SOC,e_batt_cell,'x')

% Translate from Cell level to pack level
N_series = ceil(Ubatt/Ubatt_cell_nom)
N_parallel = ceil(Wbatt/Wbatt_cell_nom/N_series)
Wbatt_nom = N_series*N_parallel*Wbatt_cell_nom;
e_batt = N_series*e_batt_cell;
Ubatt_nom = N_series*Ubatt_cell_nom;
```

```
Ibatt_max = Ibatt_cell_max*N_parallel;
Pbatt_max = Ubatt_nom*Ibatt_max
subplot(1,2,2)
plot(SOC,e_batt,'x')
```

Listing A.2: Initialization of battery parameters and calculations of the corresponding battery characteristics

```
V_to = 0;  % [V]
V_do = 0.3;  % [V]
R_t_on = 0.17e-3;   % [Ohm]
R_d_on = 0.01;  % [Ohm]

E_d_rr = 30*54e-9;  % [J]
E_on = 48*119e-9;  % [J]
E_off = 48*119e-9;  % [J]

V_dc_n = 60;  % [V]
I_n = 36;  % [A]

Udc = 48;  % [V]
P_max = 2000;  % [W]
u_phase_peak = [0:Udc/2/20:Udc/2];  % [V]
i_phase_max = P_max/(3*Udc/2)*2;  % [V]
i_phase_peak = [0:i_phase_max/30:i_phase_max];  % [A]
```

Listing A.3: Initialization of power electronic components parameters which were retrieved from the manufacturers' datasheet

```
cos_fi_values = 0.5:0.1:1;
eff = zeros(length(u_phase_peak), length(i_phase_peak), length(
    ↪ cos_fi_values));

for k = 1:length(cos_fi_values)
    cos_fi = cos_fi_values(k);
    for i=1:length(u_phase_peak)
        for j=1:length(i_phase_peak)
            P_t_sw(i,j) = 2*sqrt(2)/pi*(E_on+E_off)/(V_dc_n*I_n)*
    ↪ Udc*(i_phase_peak(j)/sqrt(2))*f_sw;
            P_d_sw(i,j) = 2*sqrt(2)/pi*E_d_rr/(V_dc_n*I_n)*Udc*(
    ↪ i_phase_peak(j)/sqrt(2))*f_sw;
            P_t_cond(i,j) = (1/2/pi*V_to*i_phase_peak(j)+1/8*
    ↪ R_t_on*(i_phase_peak(j))^2) + (1/4/pi*V_to*i_phase_peak(j)
    ↪ +1/3/pi*R_t_on*(i_phase_peak(j))^2)*u_phase_peak(i)*cos_fi
    ↪ /(Udc/2);
            P_d_cond(i,j) = (1/2/pi*V_do*i_phase_peak(j)+1/8*
    ↪ R_d_on*(i_phase_peak(j))^2) - (1/4/pi*V_do*i_phase_peak(j)
    ↪ +1/3/pi*R_d_on*(i_phase_peak(j))^2)*u_phase_peak(i)*cos_fi
    ↪ /(Udc/2);
            P_loss(i,j) = 6*(P_t_sw(i,j) + P_d_sw(i,j) + P_t_cond
    ↪ (i,j) + P_d_cond(i,j)) + P_gate;
            P_out(i,j) = u_phase_peak(i)*i_phase_peak(j)/2*3;
            eff(i,j,k) = P_out(i,j)/(P_out(i,j)+P_loss(i,j));
        end
    end
end
```

Listing A.4: Calculates the efficiency for the power electronics based on the parameters from listing A.3

```
Udc = 48;
p = 40;
Speed_vect = [0:25:650]*p/2*pi/30;   % Speed in Electric rad/s

for i=1:length(Tref_vect)
    for j=1:length(Speed_vect)

        [num2str(i) '(' num2str(length(Tref_vect)) ')  ' num2str(
    ↪ j) '(' num2str(length(Speed_vect)) ')']

        Tref = Tref_vect(i);
        Psilim = min(max(max(Psis_vect)),Udc/sqrt(2)/Speed_vect(j
    ↪ ));
        Isx_real(i,j) =  interp2(Psis_vect,Tref_vect,Isx_ref,
    ↪ Psilim,Tref);
        Isy_real(i,j) =  interp2(Psis_vect,Tref_vect,Isy_ref,
    ↪ Psilim,Tref);
        [Tref Psilim Isx_real(i,j) Isy_real(i,j)]
        slask=0;
        while isnan(Isy_real(i,j))&(slask<5)
            slask=slask+1;
            Tref = Tref*0.95;
            Isx_real(i,j) =  interp2(Psis_vect,Tref_vect,Isx_ref,
    ↪ Psilim,Tref);
            Isy_real(i,j) =  interp2(Psis_vect,Tref_vect,Isy_ref,
    ↪ Psilim,Tref);
        end
        Is_abs(i,j) = sqrt(Isx_real(i)^2+Isy_real(j)^2);
        T_act(i,j) = Tref;
        Psisx(i,j) = interp2(Isx_new,Isy_new,Psisx_new,Isx_real(i
    ↪ ,j),Isy_real(i,j));
        Psisy(i,j) = interp2(Isx_new,Isy_new,Psisy_new,Isx_real(i
    ↪ ,j),Isy_real(i,j));
        Psis(i,j) = sqrt(Psisx(i,j)^2 + Psisy(i,j)^2);
        CosPhi(i,j)=abs(cos(atan2(Psisy(i,j),Psisx(i,j))+pi/2-
    ↪ atan2(Isy_real(i,j),Isx_real(i,j))));
        Us(i,j) = sqrt((Rs*Isx_real(i,j)-Speed_vect(j)*Psisy(i,j)
    ↪ )^2 + (Rs*Isy_real(i,j)+Speed_vect(j)*Psisx(i,j))^2);

        if isnan(CosPhi(i,j)) || CosPhi(i,j) < 0.1
            CosPhi(i,j) = 1;
        end
    end
end

Us_max = max(max(Us));
Pmax = max(max(T_act.*Speed_vect*2/p))
for i=1:length(Tref_vect)
    for j=1:length(Speed_vect)
```

```
40          Ploss_resistive(i,j) = Rs.*Is_abs(i,j)^2;
41          Ploss_magnetic(i,j) = Pmax*0.02*(Psis(i,j)/max(max(Psis))
    ↪ )^2;
42          Pelectric(i,j) = -Speed_vect(j)*Psisy(i,j)*Isx_real(i,j)
    ↪ + Speed_vect(j)*Psisx(i,j)*Isy_real(i,j);
43          Paxle(i,j) = T_act(i,j)*Speed_vect(j);
44          if Paxle(i,j)>0
45              Eff(i,j) = Paxle(i,j)/(Pelectric(i,j) +
    ↪ Ploss_resistive(i,j) + Ploss_magnetic(i,j))*100;
46          else
47              Eff(i,j) = (Pelectric(i,j) + Ploss_resistive(i,j) +
    ↪ Ploss_magnetic(i,j))/Paxle(i,j)*100;
48          end
49          if abs(Paxle(i,j))>Pmax
50              Eff(i,j) = nan;
51          end
52      end
53  end
```

Listing A.5: Calculates parameters for the electric machine (based on measured data from the actual machine) and calculates its efficiency

A.2 Simulink Model

Figure A.1 presents the original Simulink model that this study was based on. This is the full model, where some of the subsystems have been modified for the model to be applicable to the LEVKART.

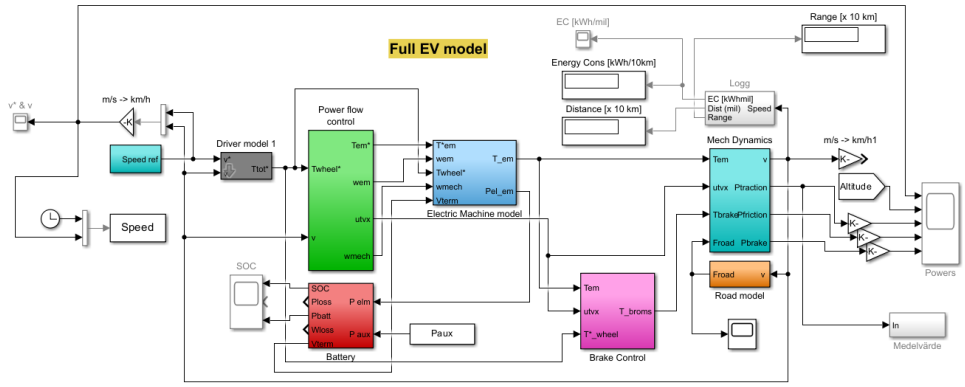

Figure A.1: The original Simulink model that this study was based upon

Figure A.2 shows the full subsystem for the battery. This is one of the subsystems which needed modifications for it to be representable for the LEVKART. The main changes include the addition of the battery voltage and the discharge curve in the calculations, which can be seen in the left part of the subsystem.

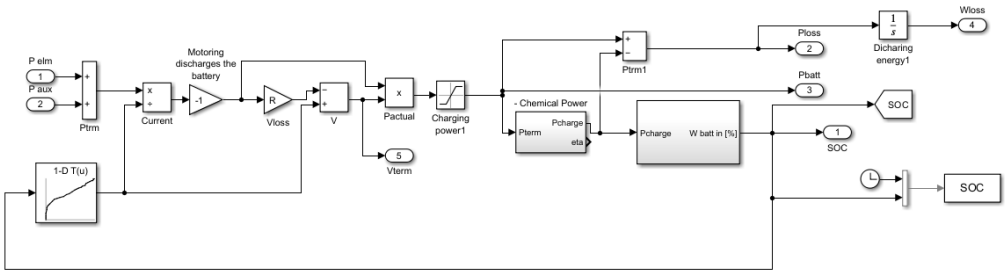

Figure A.2: The battery subsystem

One modification that was needed for the electric machine subsystem was to include calculations for the efficiency of the power electronics. This can be seen in figure A.3, which shows this addition as a part of the electric machine subsystem. In the old model, this efficiency was set to a constant 97%. It is now calculated dynamically along the entire drive cycle based on various parameters shown in figure A.3.

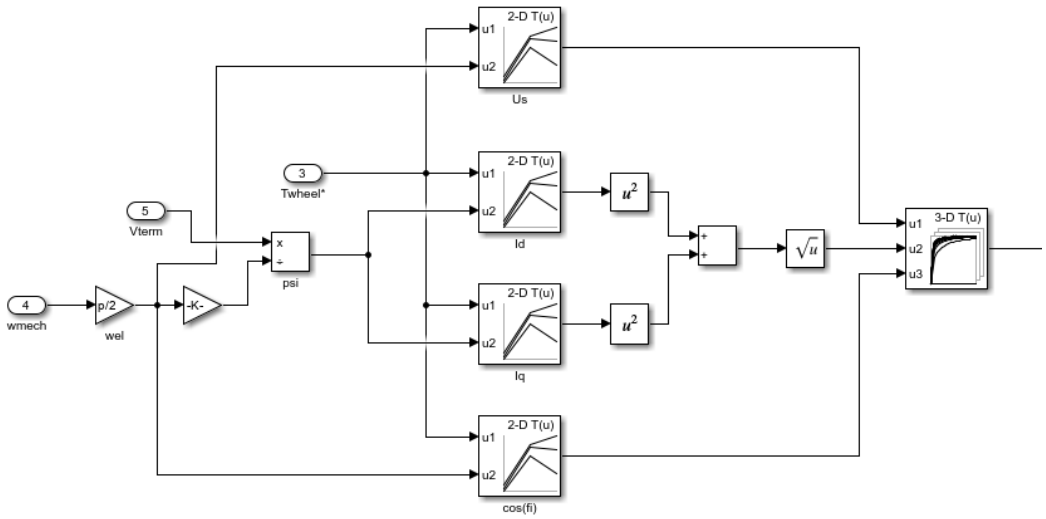

Figure A.3: Part of the subsystem for the electric machine model

Appendix B

Results and Graphs

This appendix presents in more detail the results and the resulting graphs from the simulations of the different voltage levels and different drive cycles, as well as some of the results from the tests of the electric machine

B.1 43.2 V Battery

Figures B.1, B.2 and B.3 present the resulting graphs for the LEVKART with the 43.2 V battery pack during drive cycle 1. Figure B.1 shows the velocity profile and how well the vehicle was able to follow this drive cycle, where the yellow line is the drive cycle and the blue line shows the speed of the vehicle during the simulation. Figure B.2 shows how the energy consumption varied during the drive cycle. The energy consumption is here expressed as $\frac{kWh}{10km}$. Figure B.3 shows the state of charge during the drive cycle, expressed in percentages.

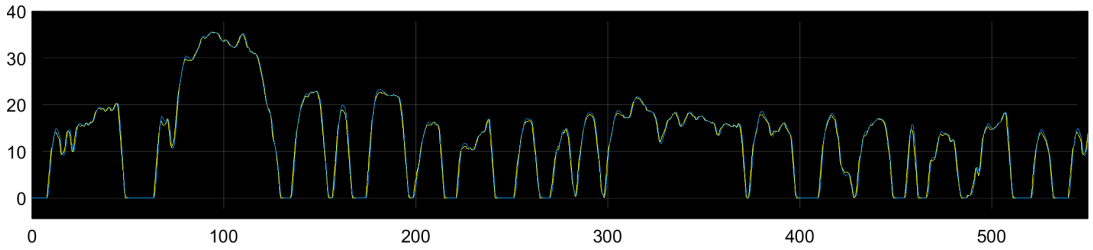

Figure B.1: Speed profile for the 43.2 V battery with drive cycle 1

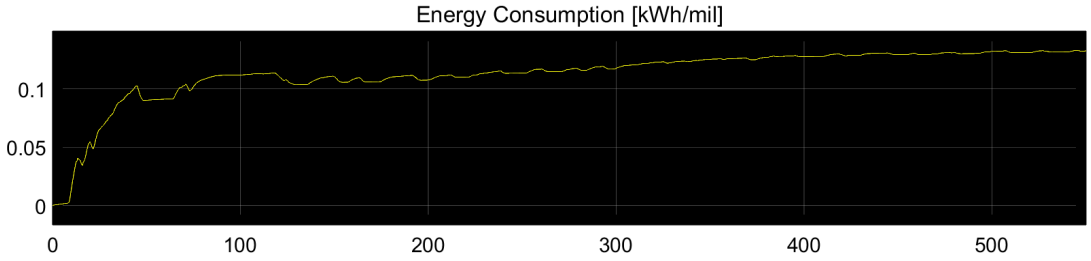

Figure B.2: The energy consumption expressed in kWh/10 km

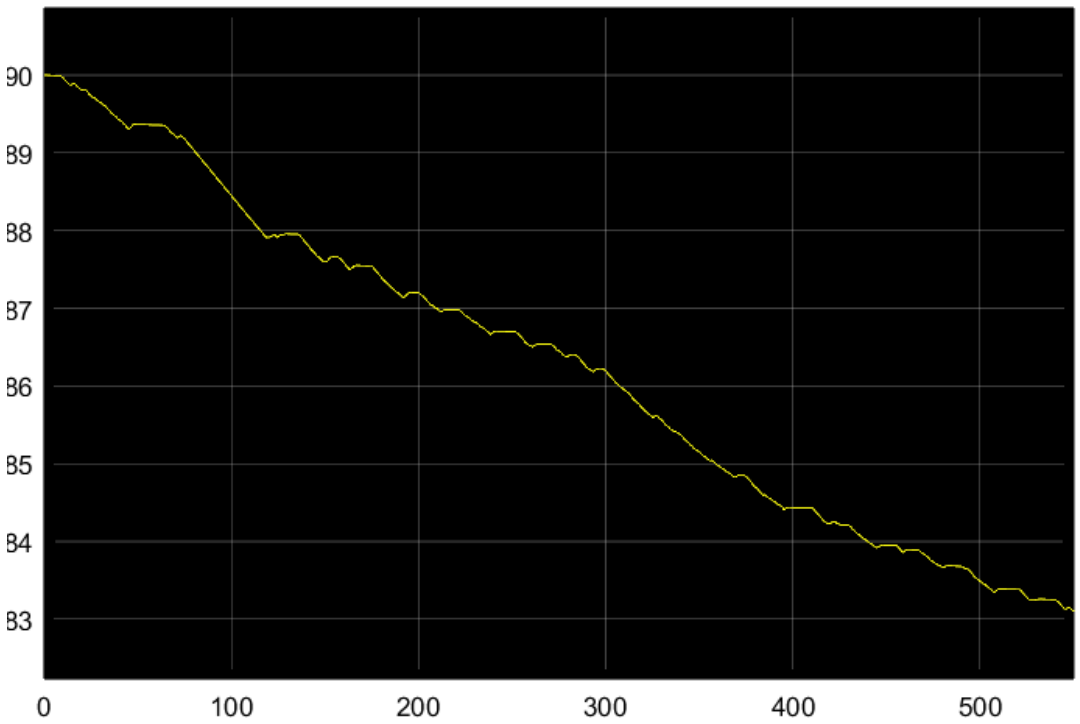

Figure B.3: State of Charge during drive cycle 1

Figure B.4 shows the cumulative losses for the 43.2 V battery during drive cycle 1. The green line shows the losses for the battery subsystem, the red line for the power electronics, the blue line for the electric machine, and the yellow line the combined losses, expressed in Wh.

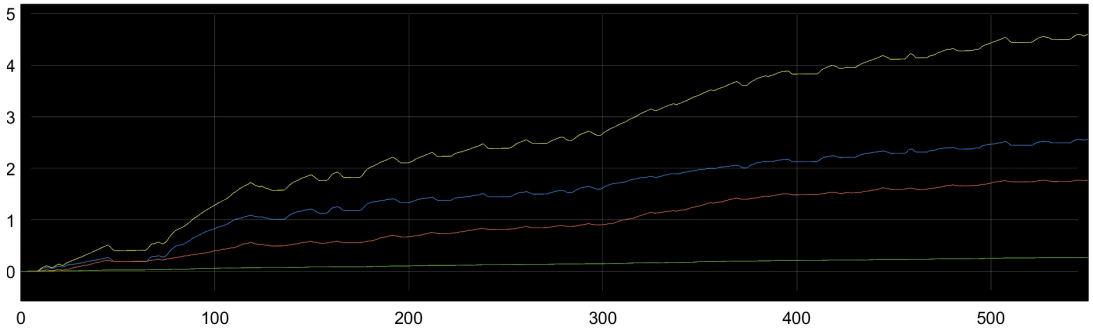

Figure B.4: Losses for the 43.2 V battery during drive cycle 1

Figures B.5, B.6, B.7, and B.8 show the resulting graphs for the LEVKART with the 43.2 V battery pack during drive cycle 2.

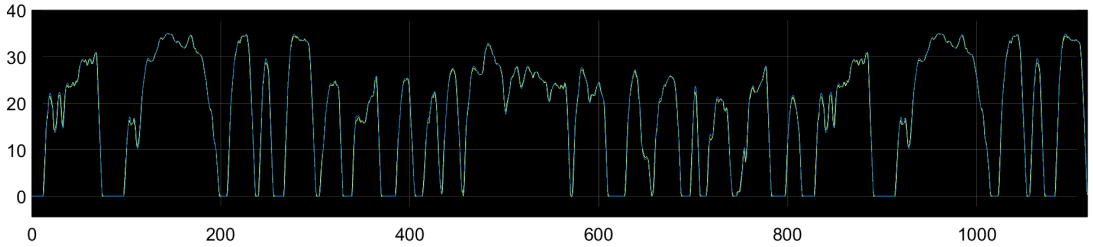

Figure B.5: Speed profile for the 43.2 V battery with drive cycle 2

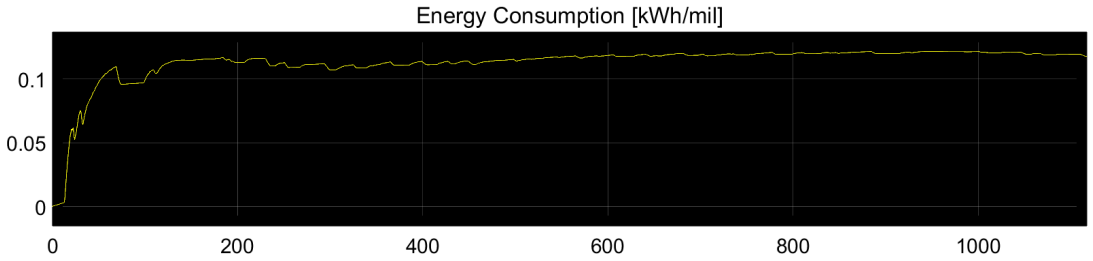

Figure B.6: The energy consumption expressed in kWh/10 km

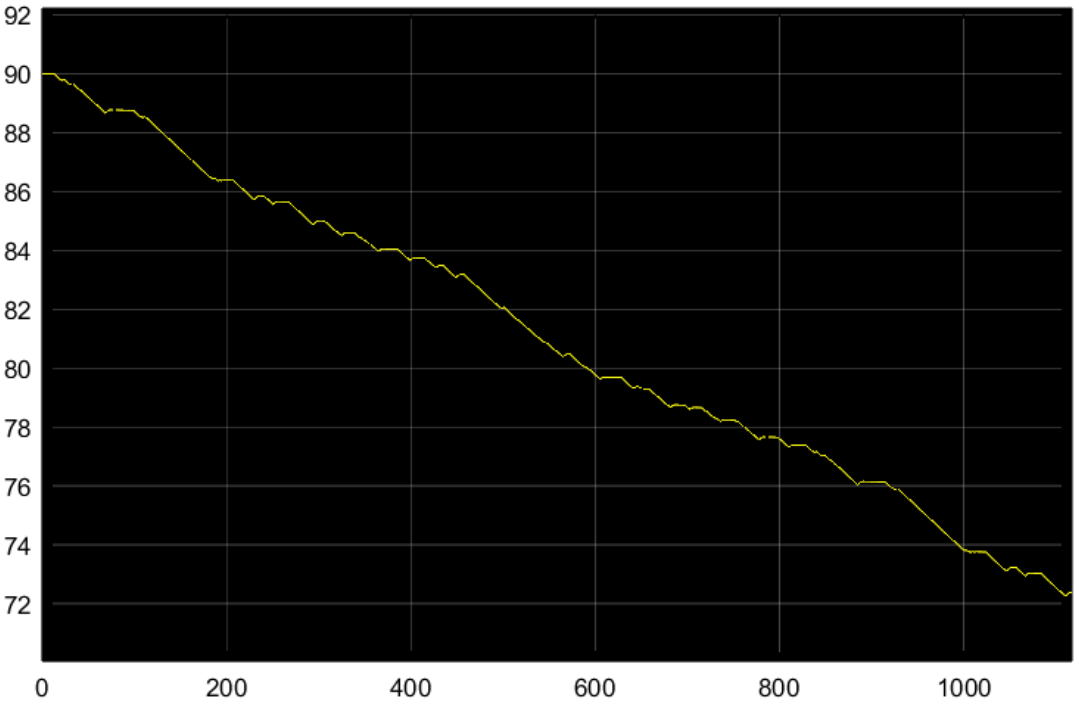

Figure B.7: State of Charge during drive cycle 2

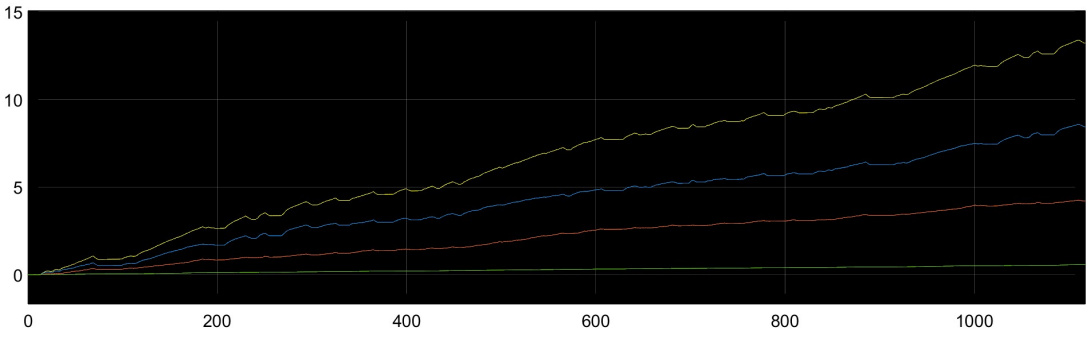

Figure B.8: Losses for the 43.2 V battery during drive cycle 2

B.2 39.6 V Battery

Figures B.9, B.10 and B.11 shows the resulting graphs for the 39.6 V battery pack during drive cycle 1, in a similar manner as for the 43.2 V simulations.

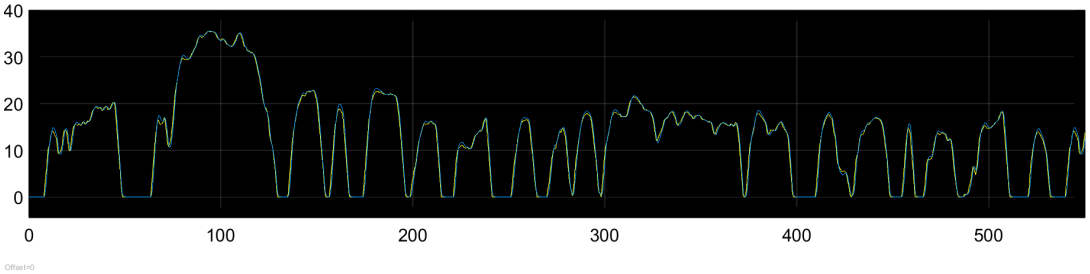

Figure B.9: Speed profile for the 39.6 V battery with drive cycle 1

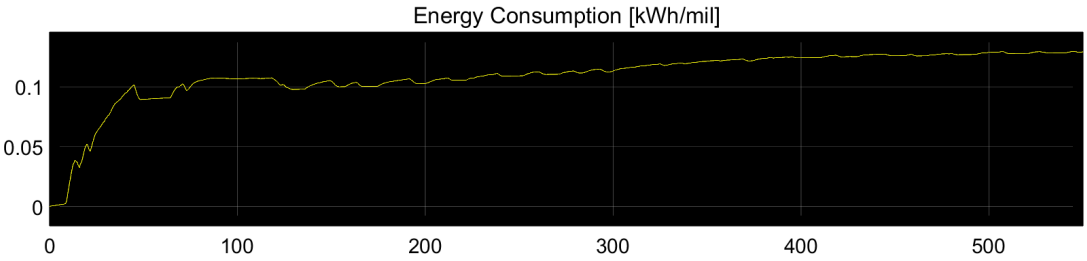

Figure B.10: The energy consumption expressed in kWh/10 km

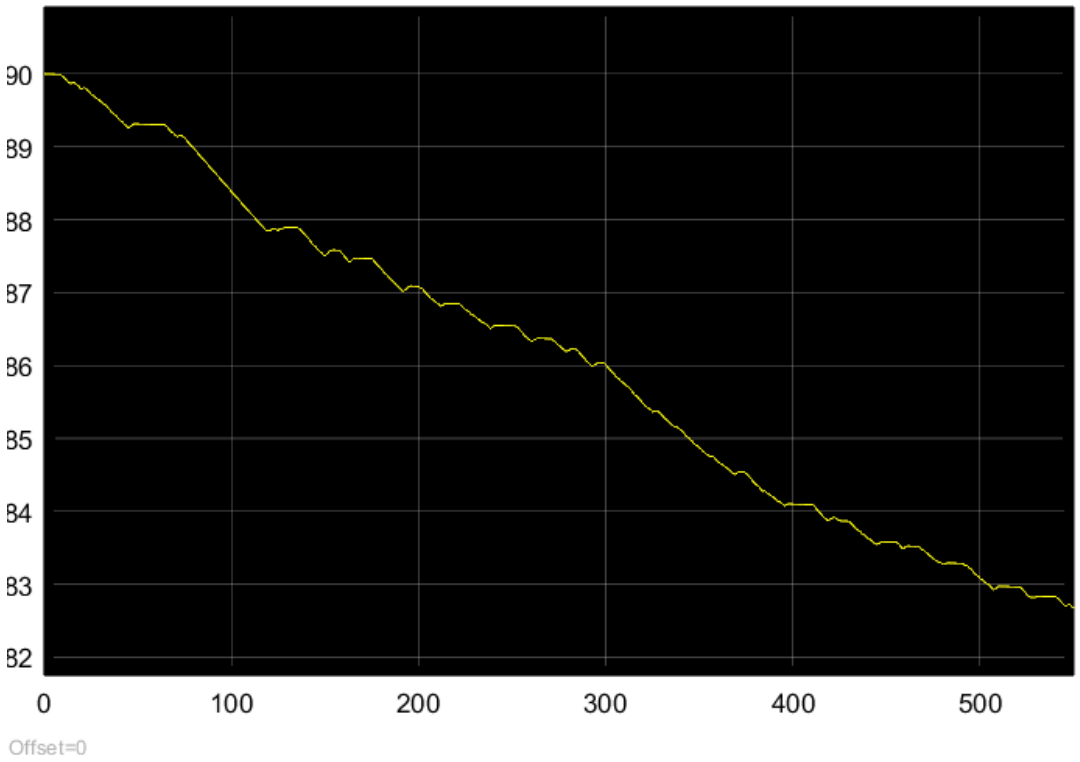

Figure B.11: State of Charge during drive cycle 1

Figure B.12 shows the cumulative losses for the 39.6 V battery during drive cycle 1, expressed in Wh. The green line shows the losses for the battery subsystem, the red line for the power electronics, the blue line for the electric machine, and the yellow line the combined losses.

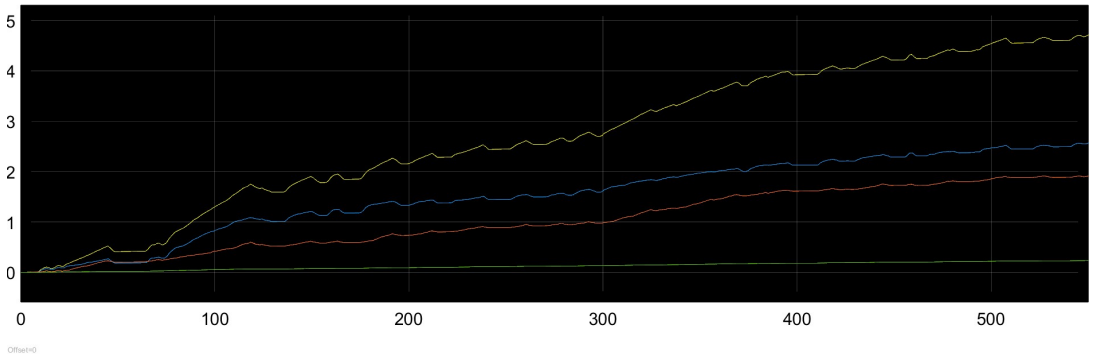

Figure B.12: Losses for the 39.6 V battery during drive cycle 1

Figures B.13, B.14, B.15, and B.16 show the resulting graphs for the 39.6 V battery pack during drive cycle 2.

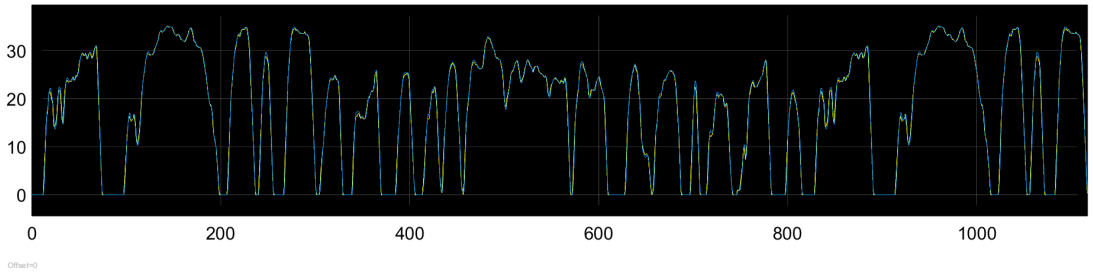

Figure B.13: Speed profile for the 39.6 V battery with drive cycle 2

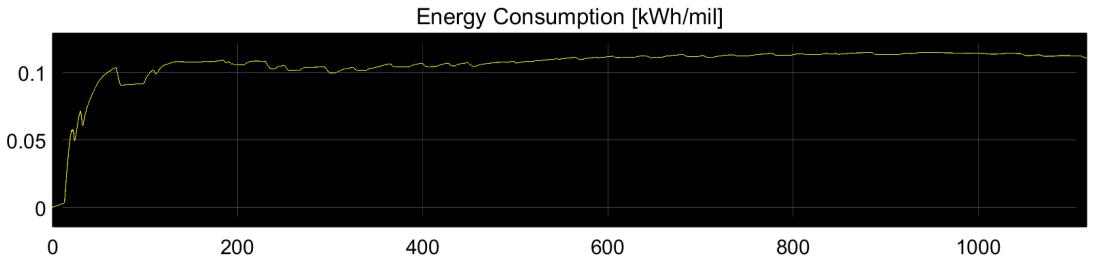

Figure B.14: The energy consumption expressed in kWh/10 km

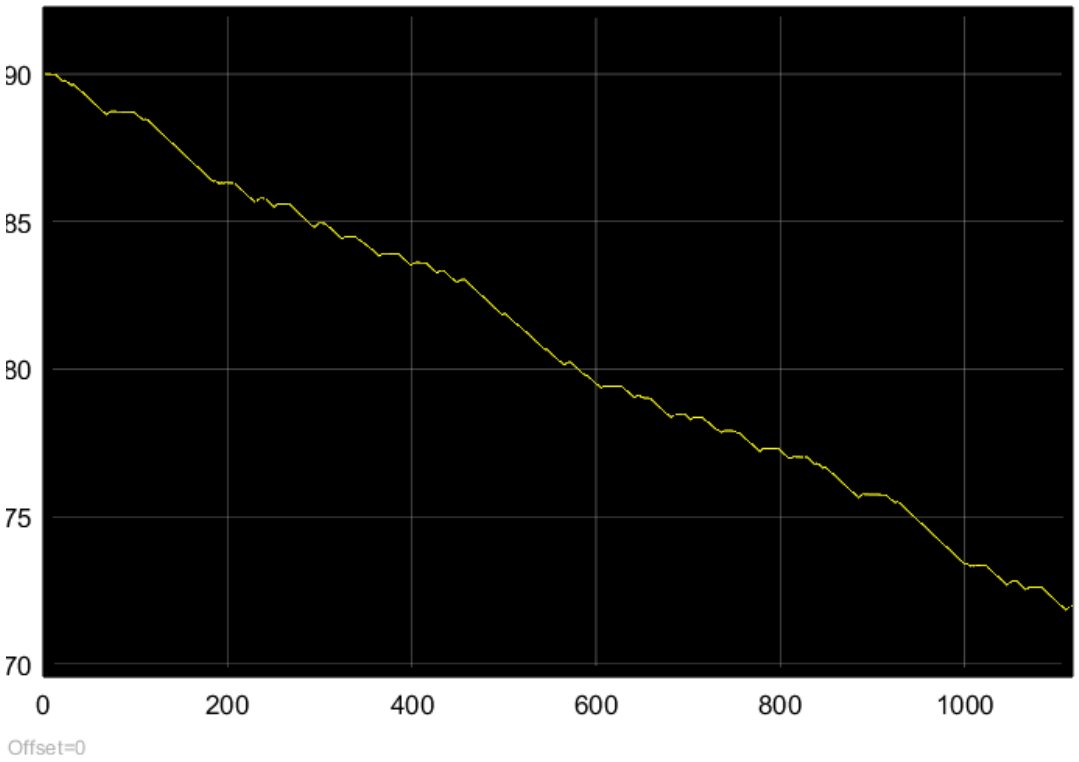

Figure B.15: State of Charge during drive cycle 2

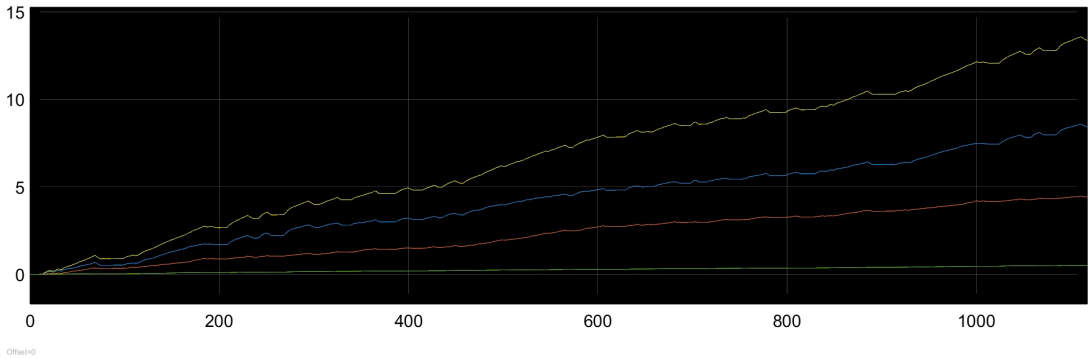

Figure B.16: Losses for the 39.6 V battery during drive cycle 2

B.3 36 V Battery

Figures B.17, B.18 and B.19 shows the resulting graphs for the 36 V battery pack during drive cycle 1, in the same way as for the 43.2 V and the 39.6 V simulations.

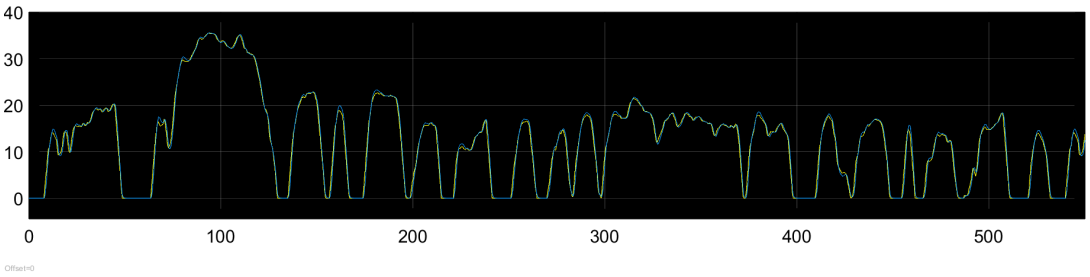

Figure B.17: Speed profile for the 36 V battery with drive cycle 1

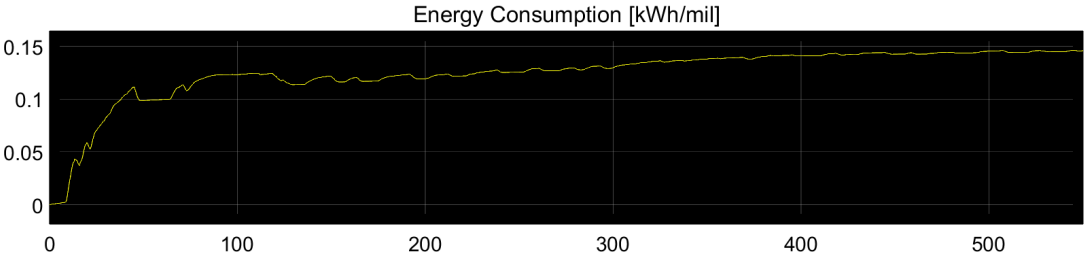

Figure B.18: The energy consumption expressed in kWh/10 km

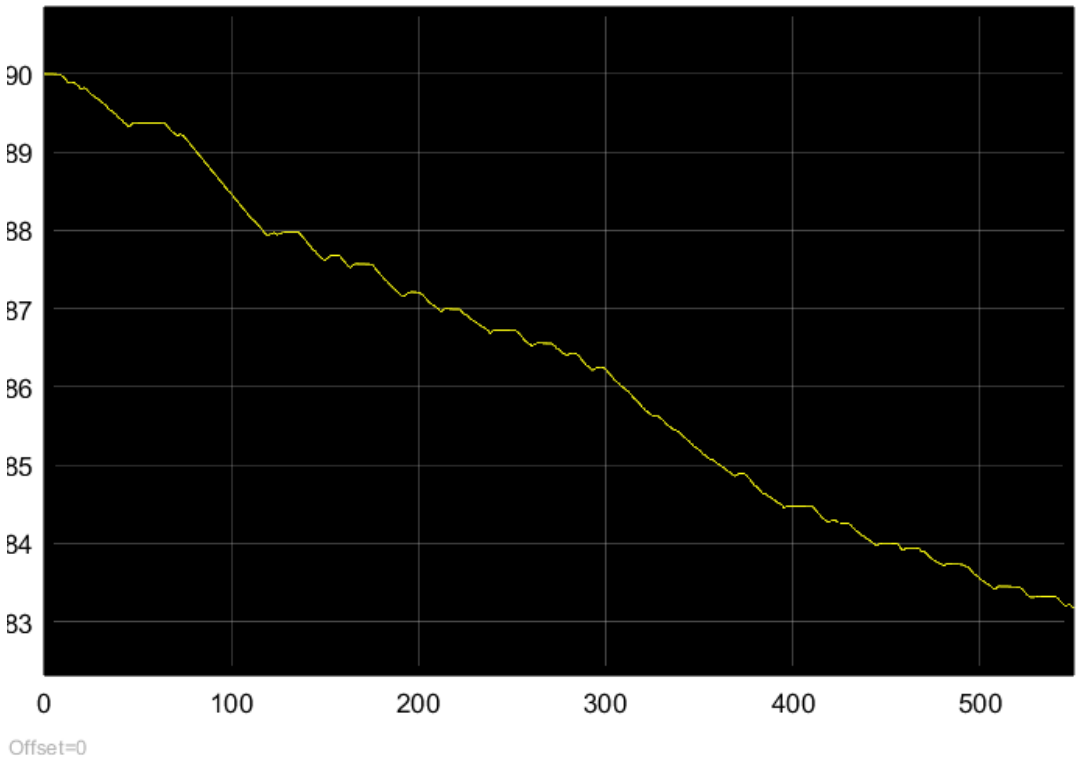

Figure B.19: State of Charge during drive cycle 1

Figure B.20 shows the cumulative losses for the 36 V battery during drive cycle 1, expressed in Wh. The green line shows the losses for the battery subsystem, the red line for the power electronics, the blue line for the electric machine, and the yellow line the combined losses.

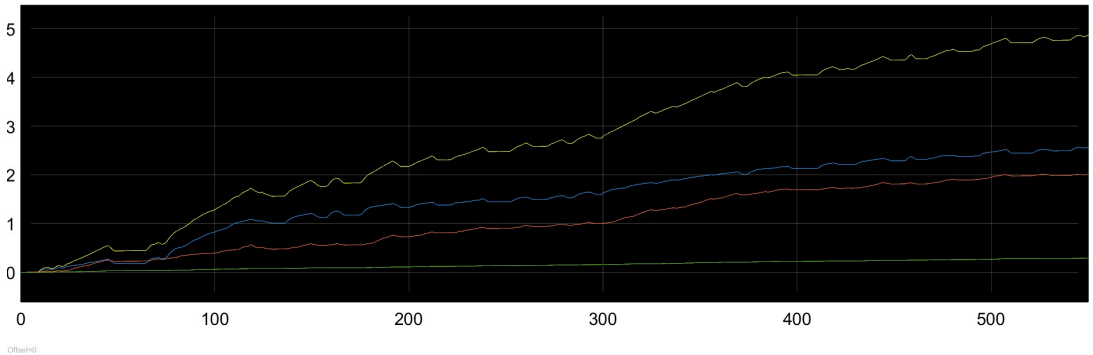

Figure B.20: Losses for the 36 V battery during drive cycle 1

Figures B.21, B.22, B.23, and B.24 show the resulting graphs for the 36 V battery pack during drive cycle 2.

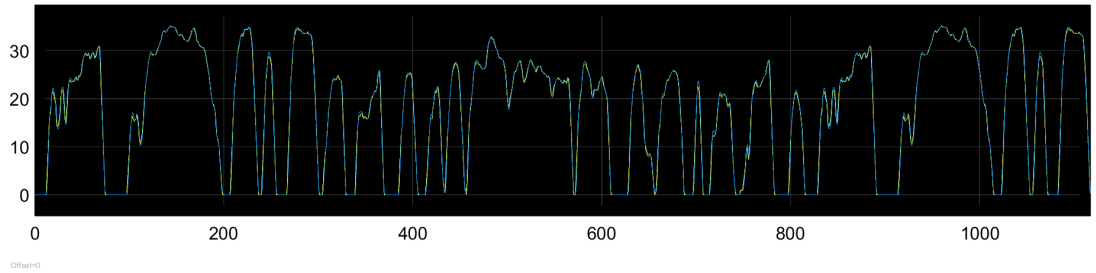

Figure B.21: Speed profile for the 36 V battery with drive cycle 2

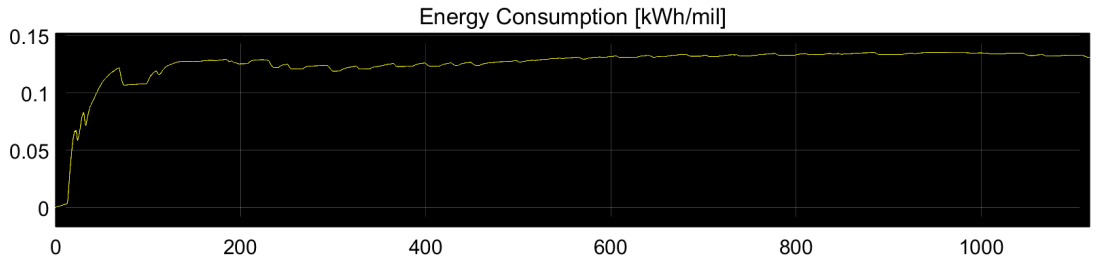

Figure B.22: The energy consumption expressed in kWh/10 km

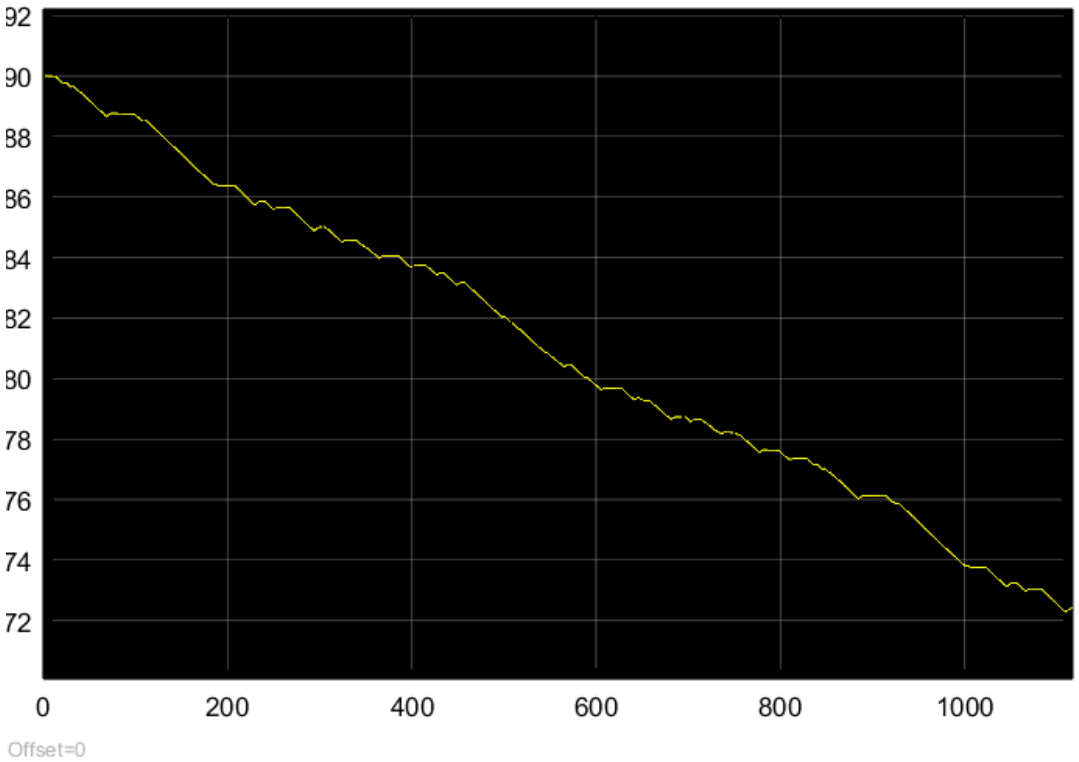

Figure B.23: State of Charge during drive cycle 2

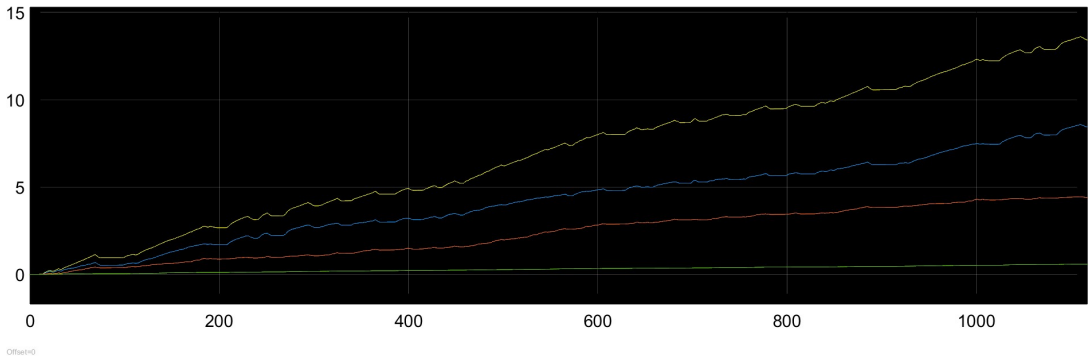

Figure B.24: Losses for the 36 V battery during drive cycle 2

B.4 Electric Machine Testing

Figures B.25, B.26, B.27, B.28, B.29, and B.30 illustrate some of the data gathered from the testing of the electric machine. The curves in each graph correspond to different applied torque values, between 1-5 Nm. The speed varies from 1000-13000 ERPM. i_{sx}, i_{sy}, u_{sx}, and u_{sy} are read from VESC Tool. ψ_{sx} and ψ_{sy} are calculated with equations 3.4 and 3.5, and the generated torque is calculated with equation 3.1, with parameters gathered from the test. The measurement of i_{sx} displayed values of zero, or very close to zero, for all speeds and applied torque values, which is why this graph is not included.

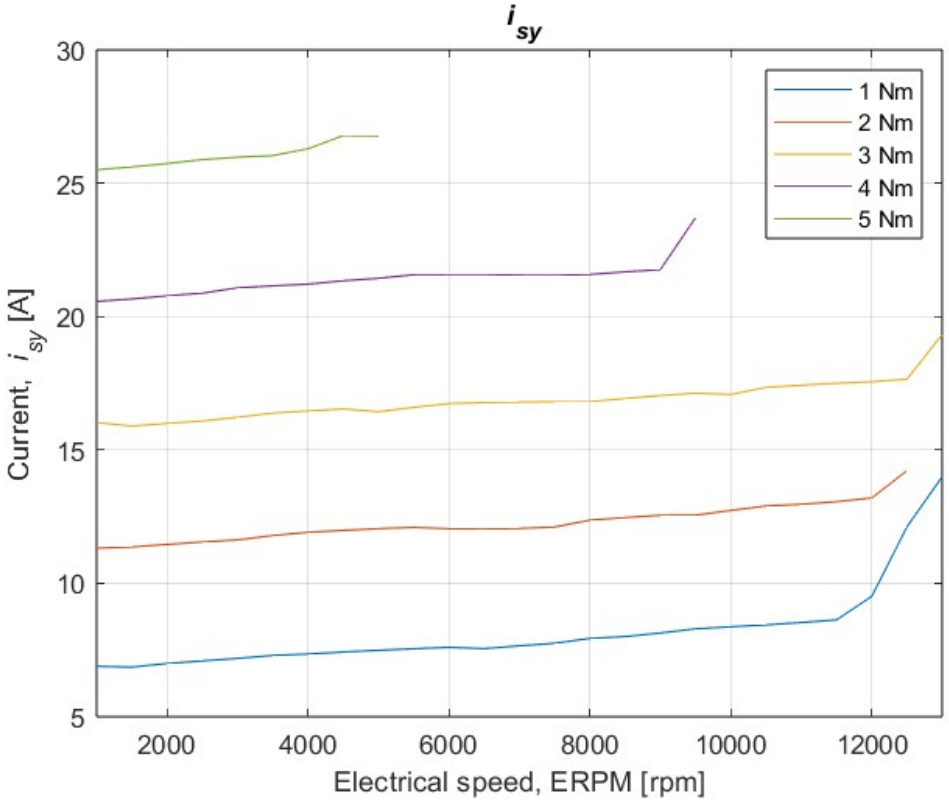

Figure B.25: Resulting i_{sy} from the tests, with an applied torque of 1-5 Nm

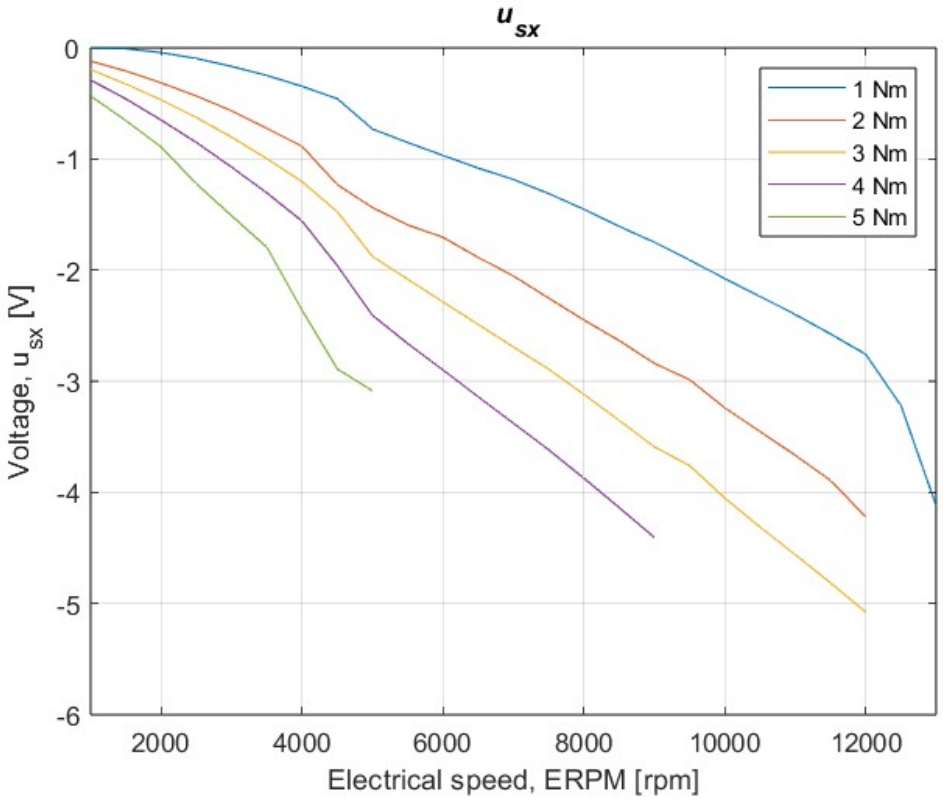

Figure B.26: Resulting u_{sx} from the tests, with an applied torque of 1-5 Nm

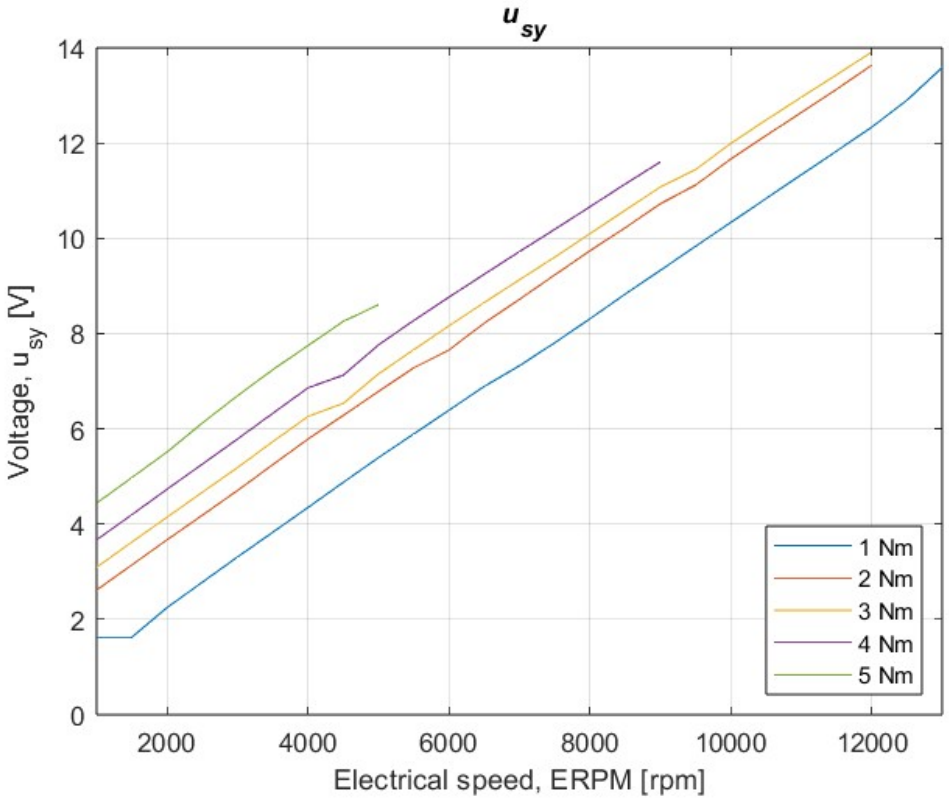

Figure B.27: Resulting u_{sy} from the tests, with an applied torque of 1-5 Nm

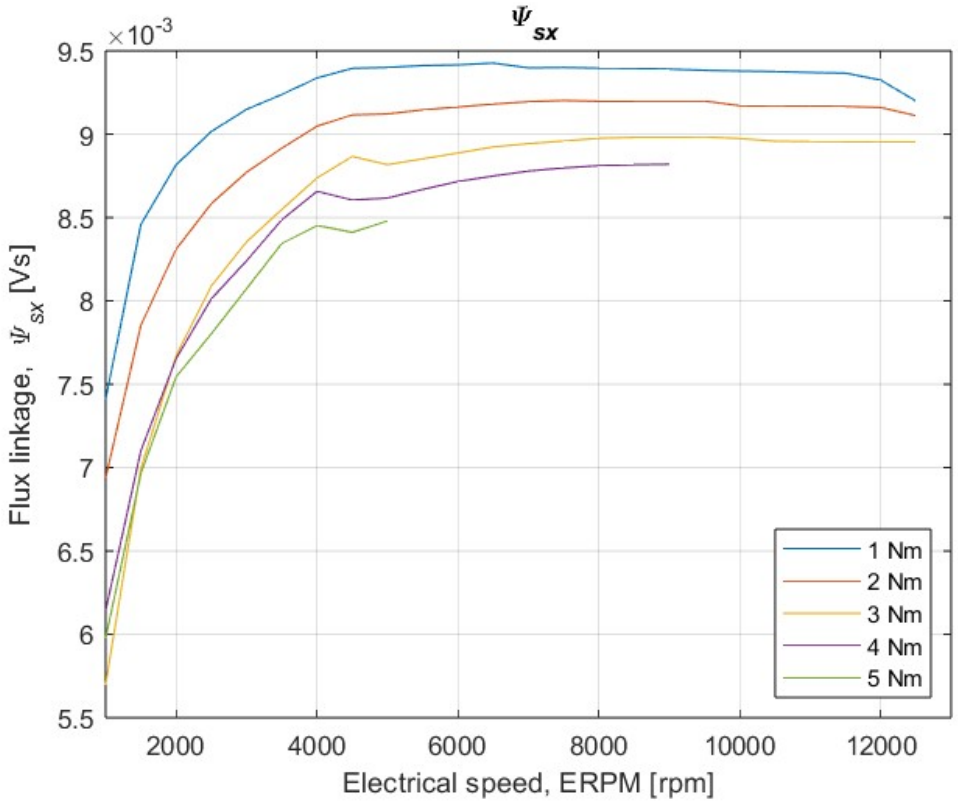

Figure B.28: Resulting ψ_{sx} from the tests, with an applied torque of 1-5 Nm

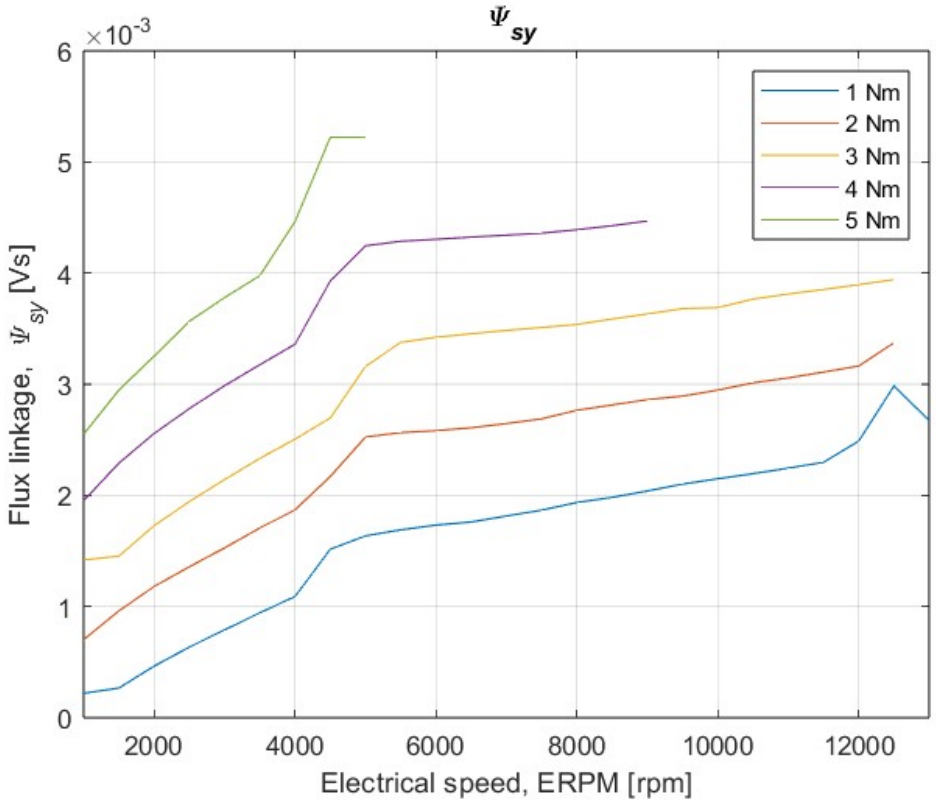

Figure B.29: Resulting ψ_{sy} from the tests, with an applied torque of 1-5 Nm

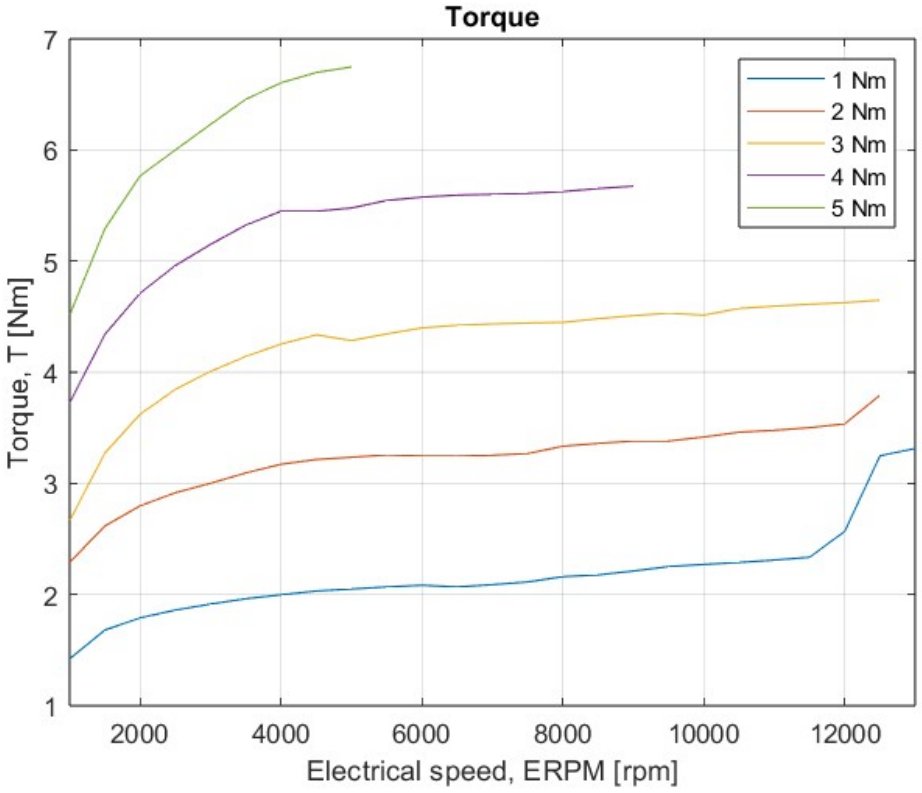

Figure B.30: Generated torque from the tests, with an applied torque of 1-5 Nm